2020

Multisystem Imaging Manifestations of COVID-19, Part 2: From Cardiac Complications to Pediatric Manifestations.

M. V. Revzin

S. Raza

N. C. Srivastava

R. Warshawsky
Zucker School of Medicine at Hofstra/Northwell

C. D'Agostino
Zucker School of Medicine at Hofstra/Northwell

See next page for additional authors

Multisystem Imaging Manifestations of COVID-19, Part 2: From Cardiac Complications to Pediatric Manifestations

Margarita V. Revzin, MD
Sarah Raza, MD
Neil C. Srivastava, MD
Robin Warshawsky, MD
Catherine D'Agostino, MD
Ajay Malhotra, MD
Anna S. Bader, MD
Ritesh D. Patel, MD
Kan Chen, MD
Christopher Kyriakakos, MD
John S. Pellerito, MD

Abbreviations: ACE2 = angiotensin-converting enzyme 2, ADC = apparent diffusion coefficient, COVID-19 = coronavirus disease 2019, FLAIR = fluid-attenuated inversion-recovery, PMIS = pediatric multisystem inflammatory syndrome, SARS-CoV-2 = severe acute respiratory syndrome coronavirus 2

RadioGraphics 2020; 40:1866–1892

https://doi.org/10.1148/rg.2020200195

Content Codes: CA CH CT

From the Department of Radiology and Biomedical Imaging, Yale University School of Medicine, 333 Cedar St, PO Box 208042, Room TE-2, New Haven, CT 06520 (M.V.R., A.M., A.S.B.); Department of Radiology, Zucker School of Medicine at Hofstra/Northwell, Northwell Health System, Manhasset, NY (S.R., R.W., C.D., R.D.P., K.C., C.K., J.S.P.); and Department of Diagnostic Radiology, Danbury Radiological Associates, PC, Danbury, Conn (N.C.S.). Received July 23, 2020; revision requested July 25 and received September 27; accepted September 27. For this journal-based SA-CME activity, the authors, editor, and reviewers have disclosed no relevant relationships. **Address correspondence to** M.V.R. (e-mail: *margarita.revzin@yale.edu*).

SA-CME LEARNING OBJECTIVES

After completing this journal-based SA-CME activity, participants will be able to:

- Describe the body system–specific pathophysiology of SARS-CoV-2.
- Discuss the most appropriate imaging modalities and radiologic recommendations for the diagnosis of nonpulmonary multisystem manifestations of COVID-19.
- Recognize key imaging features of nonpulmonary multisystem manifestations of COVID-19, as well as its manifestations in pediatric and pregnant patients.

See rsna.org/learning-center-rg.

Infection with severe acute respiratory syndrome coronavirus 2 results in coronavirus disease 2019 (COVID-19), which was declared an official pandemic by the World Health Organization on March 11, 2020. COVID-19 has been reported in most countries, and as of August 15, 2020, there have been over 21 million cases of COVID-19 reported worldwide, with over 800 000 COVID-19–associated deaths. Although COVID-19 predominantly affects the respiratory system, it has become apparent that many other organ systems can also be involved. Imaging plays an essential role in the diagnosis of all manifestations of the disease and its related complications, and proper utilization and interpretation of imaging examinations is crucial. A comprehensive understanding of the diagnostic imaging hallmarks, imaging features, multisystem involvement, and evolution of imaging findings is essential for effective patient management and treatment. In part 1 of this article, the authors described the viral pathogenesis, diagnostic imaging hallmarks, and manifestations of the pulmonary and peripheral and central vascular systems of COVID-19. In part 2 of this article, the authors focus on the key imaging features of the varied pathologic manifestations of COVID-19, involving the cardiac, neurologic, abdominal, dermatologic and ocular, and musculoskeletal systems, as well as the pediatric and pregnancy-related manifestations of the virus.

Online supplemental material is available for this article.

Introduction

The coronavirus disease 2019 (COVID-19) pandemic has affected every country in the world, and by August 2020 COVID-19 had infected over 21 million people (1,2). Although COVID-19 is well known for causing respiratory pathologic findings, it can also result in multiple extrapulmonary manifestations (3). These include myocardial dysfunction and arrhythmia, acute coronary syndromes, acute kidney injury, gastrointestinal symptoms, hepatocellular injury, hyperglycemia and ketosis, neurologic illnesses, ocular symptoms, and dermatologic complications (4). Such widespread involvement of multiple body systems is attributable to the expression of angiotensin-converting enzyme 2 (ACE2) receptors (an entry receptor for severe acute respiratory syndrome coronavirus 2 [SARS-CoV-2]) in multiple extrapulmonary tissues, resulting in direct viral tissue damage. This virus is responsible for initiation of endothelial damage and thromboinflammation and dysregulation of immune responses, all of which contribute to the development of extrapulmonary manifestations (4). In part 1 of this article, we provided a detailed discussion of the pathophysiology of the virus and its pulmonary and vascular manifestations (5).

TEACHING POINTS

- Although COVID-19 is well known for causing respiratory pathologic findings, it can also result in multiple extrapulmonary manifestations. These include myocardial dysfunction and arrhythmia, acute coronary syndromes, acute kidney injury, gastrointestinal symptoms, hepatocellular injury, hyperglycemia and ketosis, neurologic illnesses, ocular symptoms, and dermatologic complications.
- SARS-CoV-2 infection can cause detrimental effects on the cardiovascular system and result in complications that include myocardial injury, arrhythmia, arterial and venous thromboembolism, myocarditis, cardiomyopathy, cardiogenic shock, and cardiac arrest.
- There is increasing evidence of neurologic manifestations associated with COVID-19, including acute stroke (6%) and altered mental status (15%). Other neurologic manifestations include epilepsy, disturbed consciousness, encephalopathy, and headache.
- Solid organ infarcts may also be visualized at abdominal imaging in patients with COVID-19, affecting the kidney, spleen, and liver. In a recent study of 141 patients who underwent abdominopelvic CT, 18% had solid organ infarcts.
- According to the American College of Radiology Appropriateness Criteria, imaging is not indicated in a well-appearing immunocompetent child older than 3 months of age who does not require hospitalization. However, if the child is not responding to outpatient management or requires hospitalization, chest radiography is considered the most appropriate first step in imaging evaluation.

In this article, we focus on extrapulmonary imaging manifestations of COVID-19, specifically those involving the cardiac, neurologic, abdominal, dermatologic, ocular, and musculoskeletal systems. We also discuss pediatric manifestations of the virus and COVID-19 in pregnant patients. The familiarity of radiologists with the spectrum of multisystem imaging manifestations of the virus will ensure prompt diagnosis and thereby facilitate appropriate care to patients and thus improve their recovery from the infection. A thorough knowledge of the available modalities and pandemic-safe imaging algorithms is paramount to properly manage patients with COVID-19 and optimize detection of COVID-19–related complications (Fig 1).

Cardiac Manifestations

There has been growing recognition that patients with underlying cardiovascular disease, including hypertension, diabetes mellitus, and obesity, may be disproportionally affected by SARS-CoV-2 and experience a greater severity of disease, worse prognosis, and higher risk of mortality (6,7). SARS-CoV-2 infection can cause detrimental effects on the cardiovascular system and result in complications that include myocardial injury, arrhythmia, arterial and venous thromboembolism, myocarditis, cardiomyopathy, cardiogenic shock, and cardiac arrest (8). Myocardial injury occurs in 20%–30% of hospitalized patients with COVID-19, with higher rates (55%) among those with preexisting cardiovascular disease (6,9). Biventricular cardiomyopathy has been reported in 7%–33% of critically ill patients with COVID-19 (10), and fulminant myocarditis was suspected in 7% of patients with lethal outcome (7).

Myocardial injury, characterized by elevated serum troponin levels, is associated with severe disease and higher mortality and can be caused by acute coronary syndrome, demand ischemia, injury owing to disseminated intravascular coagulation, myocarditis, stress-induced cardiomyopathy, or cytokine release syndrome.

Several potential mechanisms of viral-induced myocardial injury have been described. Severe viral infection can increase the risk of plaque rupture and coronary thrombosis, resulting in myocardial infarction. Severe infection can also cause hypoxemia and vasoconstriction and, particularly in the setting of sepsis, lead to a decrease in oxygen supply to the myocardium. This sustained supply-demand mismatch can lead to myocardial ischemia, especially in patients with underlying atherosclerotic disease. Lastly, if disseminated intravascular coagulation occurs in the setting of severe sepsis, resultant systemic thrombosis can affect the epicardial coronary arteries, as well as the microvasculature, leading to ischemia, focal myocardial necrosis, and severe cardiac dysfunction. Nonischemic myocardial injury can occur in the setting of myocarditis and stress-induced cardiomyopathy, with occurrence of acute heart failure in those without a history of ventricular dysfunction (11).

Imaging plays an important role in early diagnosis of disease in patients with underlying cardiovascular conditions, as well as detection of cardiovascular complications in those with an established SARS-CoV-2 infection. Although signs of cardiac failure can be readily evaluated at chest radiography, chest CT, and echocardiography, myocardial injury can be best assessed using cardiac MRI.

A typical MRI protocol would include performing at least *(a)* short-axis cine imaging to determine cardiac size and function, *(b)* T2-weighted imaging, *(c)* delayed postcontrast (after the administration of contrast material) imaging, and *(d)* T1 and T2 mapping, if possible. Emerging evidence of the high prevalence of cardiac involvement in patients with COVID-19 justifies the need for performing MRI in this patient population. In fact, in a recent cohort study of 100 patients who recovered from COVID-19, cardiac MRI helped confirm cardiac involvement in 78 patients (78%) and ongoing myocardial inflammation in 60 patients (60%). These findings were

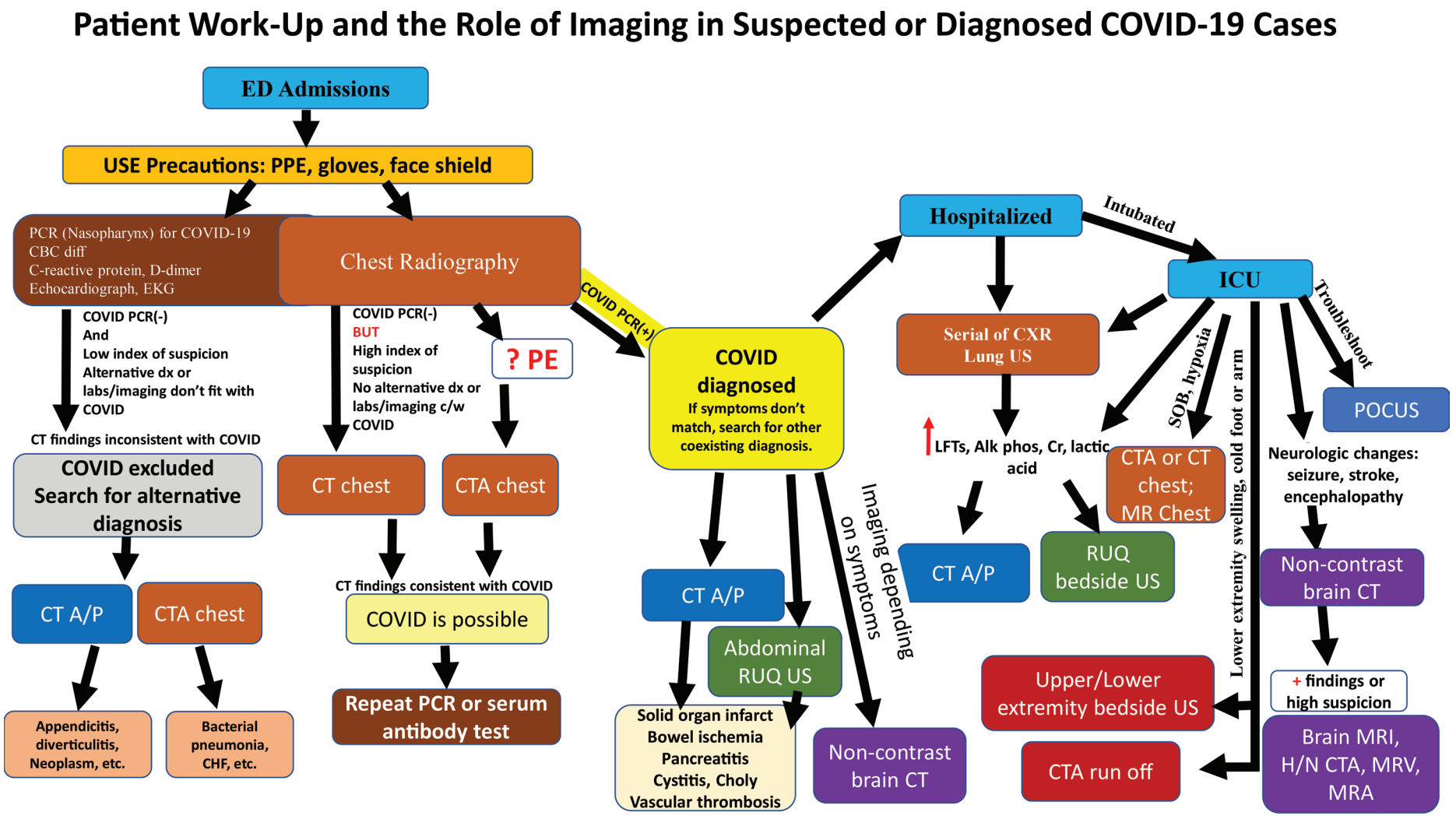

Figure 1. Flow chart shows the suggested patient workup and role of imaging in COVID-19. *Alk phos* = alkaline phosphatase, *c/w* = consistent with, *CBC diff* = complete blood count with differential, *CHF* = congestive heart failure, *Choly* = cholecystitis, *Cr* = creatinine, *CT A/P* = CT of the abdomen and pelvis, *CTA* = CT angiography, *CXR* = chest radiography, *dx* = diagnosis, *ED* = emergency department, *EKG* = electrocardiography, *H/N CTA* = head and neck CT angiography, *ICU* = intensive care unit, *LFT* = liver function tests, *MRA* = MR angiography, *MRV* = MR venography, *PE* = pulmonary embolism, *PCR* = polymerase chain reaction, *POCUS* = point-of-care US, *PPE* = personal protective equipment, *RUQ* = right upper quadrant, *SOB* = shortness of breath, *(-)* = negative, *(+)* = positive.

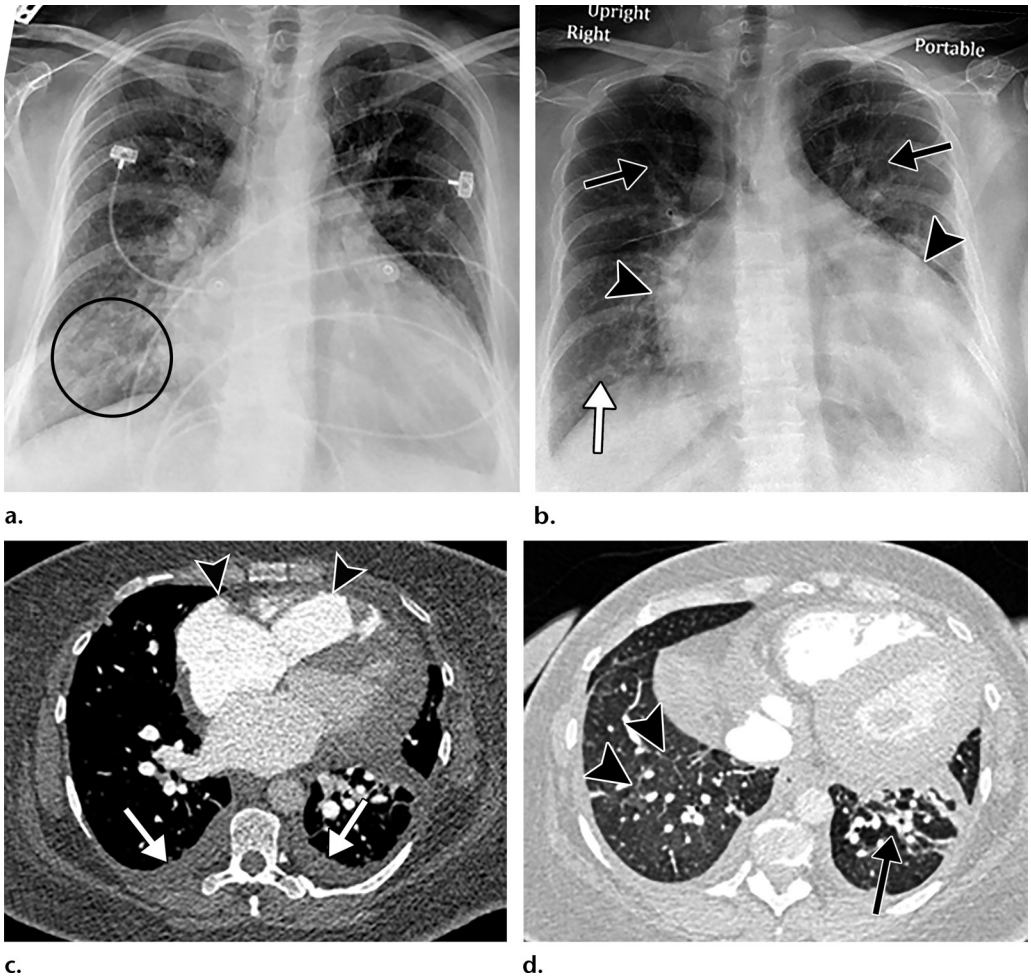

Figure 2. Pulmonary edema in a 50-year-old woman with a history of end-stage renal disease who underwent hemodialysis and who was admitted to the hospital for hypoxia and pneumonia in the setting of COVID-19. **(a)** Upright posteroranterior chest radiograph obtained at hospital admission shows a right lower lobe consolidation (circle). **(b–d)** Chest radiograph **(b)** and axial contrast material–enhanced chest CT images **(c, d)** obtained after 1 month for persistent hypoxemia show pulmonary edema (with pulmonary venous congestion [black arrows in **b**] depicted on the chest radiograph), increasing small bilateral pleural effusions (arrows in **c**), cardiomegaly (arrowheads in **b** and **c**), prominent interlobular septal (arrowheads in **d**) and peribronchovascular (arrow in **d**) thickening, and diffuse ground-glass opacities. The findings are indicative of pulmonary edema superimposed on the typical appearance of COVID-19 pneumonia. Note that the right lower lobe pneumonia depicted in **a** is almost completely resolved in **b** (white arrow in **b**).

independent of preexisting conditions, the severity and overall course of acute illness, and the time from the original diagnosis (11). However, cardiac MRI may be deferred in patients with elevated troponin levels or suspected myocardial injury related to myocarditis, owing to risk-benefit concerns related to infection control measures (12). Therefore, determining an accurate diagnosis can be challenging if cardiac MRI or biopsy is not available during the pandemic.

The development of heart failure in patients with COVID-19 can be monitored at routine chest radiography. Superimposed pulmonary edema in the setting of viral pneumonia can manifest on chest radiographs as vascular congestion, perihilar and interstitial edema, diffuse hazy or ground-glass opacities, and pleural effusions (Fig 2). At CT, findings include interlobular septal thickening, peribronchovascular prominence, diffuse ground-glass opacities, bilateral pleural effusions, and cardiomegaly (Fig 2). If contrast material is administered, the reflux of contrast material into the inferior vena cava and hepatic veins can suggest the presence of right heart failure. On chest radiographs and CT images, one should note findings of atherosclerotic disease and/or signs of prior myocardial infarction (if the patient's history is unavailable), including ventricular aneurysm, myocardial thinning, and fatty metaplasia and calcification of a post–myocardial infarction scar.

In suspected cases of myocarditis, cardiac MRI can be performed (8). Classic MRI features of myocarditis include regional or global wall motion abnormalities at steady-state free-precession

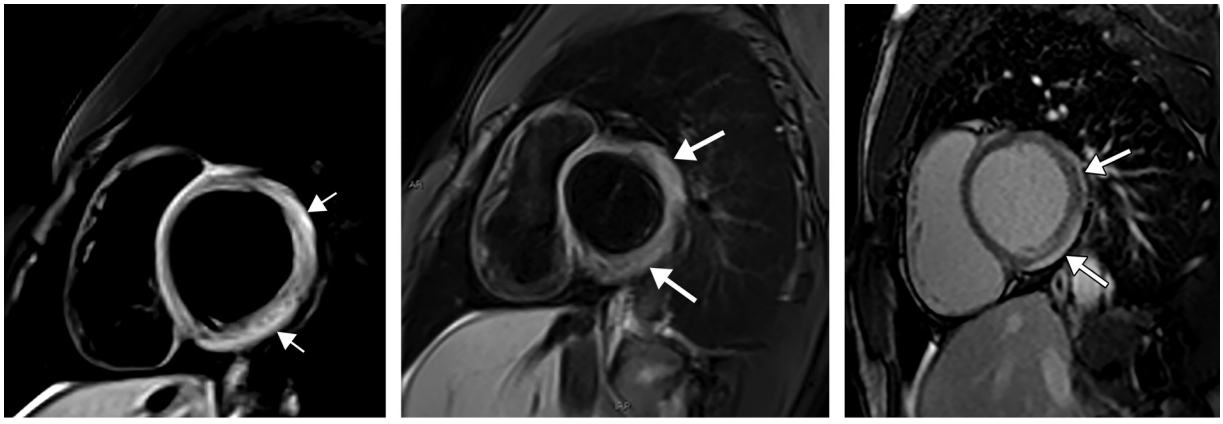

a. b. c.

d.

Figure 3. Myocarditis in a 17-year-old adolescent boy who presented to the pediatric emergency room with chest pain and was diagnosed with elevated troponin levels, diffuse ST-segment elevation at electrocardiography, ventricular ectopy, and COVID-19. **(a)** Cardiac short-axis T2-weighted fat-saturated black-blood MR image shows diffuse increased signal intensity in the subepicardial layer of the septal, lateral, and inferolateral walls in the basal segment (arrows) and subepicardial layer of the lateral and inferolateral walls of the midventricular segments (not shown), consistent with edema. **(b)** Precontrast T1-weighted short-axis fat-saturated MR image shows normal myocardial thickness and signal intensity (arrows). **(c, d)** Postcontrast short-axis T1-weighted cardiac MR images obtained at the same level as **b** show early **(c)** and delayed **(d)** subepicardial enhancement of the basal anterior, anterolateral, inferolateral, and inferior segments in a nonischemic pattern (arrows), findings consistent with myocarditis given the clinical context. The enhancement area corresponds to the T2 signal abnormality depicted in **a**.

(SSFP) cine imaging, a diffuse increase in T1 relaxation times at T1 mapping, and late gadolinium enhancement in a nonischemic pattern, typically with subepicardial enhancement in a nonvascular distribution (midmyocardial and transmural enhancement is visualized less frequently). In acute myocarditis, characteristic signal hyperintensity is observed at black-blood T2-weighted sequences, representing cardiac edema (Fig 3) (12,13). Myocardial edema and/or scarring have been observed at cardiac MRI in all of the SARS-CoV-2–related myocarditis cases for which cardiac MRI interpretation results were reported (12–14).

Cardiomyopathy is a common complication of SARS-CoV-2 infection and may result from myocarditis, profound systemic inflammation, and/or microvascular dysfunction. A case series study showed that 67% of critically ill patients with COVID-19 required treatment with vasopressor medication and that 33% developed cardiomyopathy (15). It is important to note that cardiomyopathy can occur with mild or absent respiratory symptoms. Chest radiographs may show cardiomegaly and signs of acute congestive failure, which manifest with cephalization of pulmonary vessels, pleural effusion, and Kerley B lines (Fig 2). Cardiac CT or MRI may show dilated ventricles, decreased ejection fraction, and MRI signs of myocarditis (as discussed previously) (Movie 1). (16).

Cardiomyopathy and myocarditis in severe or critically ill COVID-19 cases could contribute to the development of cardiac arrhythmias, including atrial fibrillation. Atrial fibrillation was a cause of fatality in 6.8% of patients with COVID-19 in Italy (17). The hypercoagulable state associated with COVID-19 also significantly contributes to the development of central vascular thrombosis (5). Attention to the cardiac chambers and appendages, as well as the thoracic aorta, should be made at CT angiography to avoid missing a cardiac thrombosis and potential source of embolism in abdominal vasculature, peripheral arterial vessels, and elsewhere (Fig 4, E1).

Neurologic Manifestations

There is increasing evidence of neurologic manifestations associated with COVID-19, including acute stroke (6%) and altered mental status (15%) (18). Other neurologic manifestations include epilepsy, disturbed consciousness, encephalopathy, and headache (19). Various pathophysiologic mechanisms of neurologic sequelae have been proposed, including injury to the vascular endothelial and epithelial cells, resulting in disruption of the blood brain barrier; hypoxic injury owing to respiratory failure (acute respiratory distress syndrome [ARDS]) and prolonged ventilation; ACE2 receptor–facilitated entry of the virus into neural tissue cells; and immune injury secondary to cytokine storm syndrome

Figure 4. Right ventricular thrombus and COVID-19 pneumonia in a 62-year-old man with hypoxia and markedly elevated D-dimer levels (>50 000 ng/mL). Axial chest CT angiographic image shows a well-circumscribed hypoattenuating filling defect within the lumen of the right ventricle, indicative of a thrombus (solid arrow). Patchy lung opacities (dashed arrows) related to COVID-19 pneumonia are only vaguely depicted, owing to the window settings used.

(19–21). In fact, the neurotropism of coronavirus may indeed be responsible for the relatively high percentage of neurologic involvement in this group (22,23). In addition, SARS-CoV-2–induced coagulopathy significantly contributes to the development of neurologic manifestations in patients with COVID-19 (18,19,24).

Patients with COVID-19 who present with neurologic or psychiatric symptoms may undergo nonenhanced CT of the head to identify potential vascular complications such as stroke, hemorrhage, or venous sinus thrombosis. In the setting of a suspected infarct, nonenhanced MRI of the brain can be performed for definitive assessment. Abbreviated MRI protocols can be adopted in this setting, limited to the acquisition of critical sequences such as diffusion-weighted imaging and corresponding apparent diffusion coefficient (ADC) mapping, as well as axial T2-weighted fluid-attenuated inversion-recovery (FLAIR) sequences. The use of contrast material can be helpful in imaging patients with suspected viral encephalitis to assess for potential leptomeningeal enhancement.

About one-third of patients with acute or subacute COVID-19 referred for neuroimaging may show brain abnormalities (25). The results of a large multi-institutional study in France showed ischemic strokes depicted in 27% of patients, leptomeningeal enhancement in 17%, and encephalitis in 13% (26). Large infarcts have been reported in 45% of patients, with lacunar infarcts in 24% and hemorrhagic stroke in another 24% of 38 patients with COVID-19 from a large cohort within the New York health system (27).

A wide spectrum of imaging findings has been described in patients with COVID-19. The results of a recent study with a large nationwide cohort revealed the most common imaging finding to be unilateral FLAIR and/or diffusion hyperintensities in the mesial temporal lobe (depicted in 43%) (28). These may be due to infectious versus autoimmune encephalitis. Nonconfluent multifocal white matter hyperintense lesions associated with hemorrhagic lesions have been reported in 30%, in a pattern similar to that in acute disseminated encephalomyelitis or acute hemorrhagic leukoencephalitis (28,29). Extensive and isolated white matter microhemorrhages were depicted in up to 24%, in a pattern reminiscent of disseminated intravascular coagulation (28,30).

Patients may have extensive and confluent supratentorial white matter hyperintensities at FLAIR imaging or nonconfluent multifocal white matter FLAIR hyperintense lesions. T2-hyperintense lesions have also been reported uncommonly in the splenium of the corpus callosum and in the bilateral middle cerebellar peduncles (28). The potential explanation for white matter hyperintense lesions may include viral encephalitis, postinfectious demyelination, delayed posthypoxic leukoencephalopathy, metabolic or toxic encephalopathy, or posterior reversible encephalopathy syndrome (28–31). Acute necrotizing encephalopathy may be found uncommonly, with hemorrhagic rim-enhancing lesions within the bilateral thalami, medial temporal lobes, and subinsular regions (32). Up to 25% of patients may have a combination of two or more imaging patterns (28).

There are multiple reports that describe other neurologic manifestations such as sudden loss of taste (hypogeusia) or smell (hyposmia, anosmia), implying that the viral central nervous system invasion in COVID-19 is possible through a retrograde neuronal route, with direct damage to the olfactory and gustatory receptors (33,34).

Assessment of the main intracranial vessels for hyperattenuation (eg, hyperattenuating middle cerebral artery sign) at nonenhanced CT is essential for the diagnosis of a large vessel occlusion. Embolic infarcts depicted as multiple areas of hypoattenuation in the white matter–gray matter junction can be identified and are reflective of thromboembolization, specifically cardiothromboembolism or arterio-arterial embolization (Figs 5, 6) (35). Watershed infarcts between arterial territories can be found in patients with hypoperfusion (Fig 7). Posterior reversible encephalopathy syndrome should be suspected with signal intensity changes seen at MRI or areas of hypoattenuation seen at CT in the parieto-occipital white matter, especially in a setting of

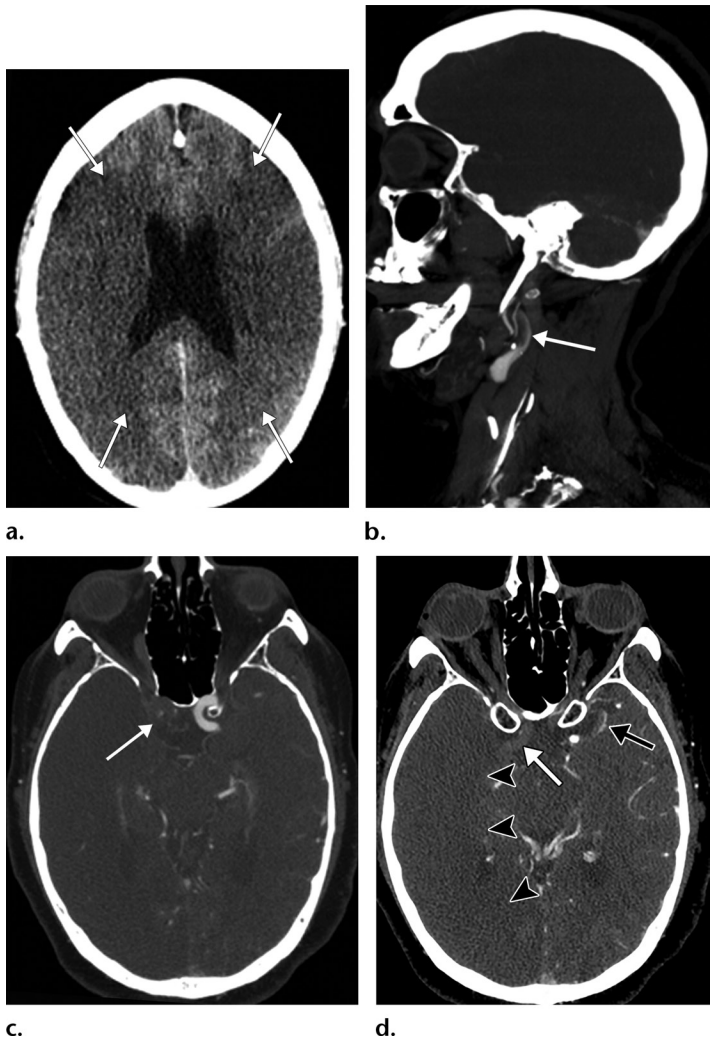

Figure 5. Long segment right internal carotid artery (ICA) occlusion with associated bilateral large middle cerebral artery territory infarcts in a 59-year-old man who underwent intubation due to COVID-19 who presented with sudden onset of confusion. The serum analysis results showed a high D-dimer level of 5.6 mg/mL. **(a)** Axial nonenhanced head CT image shows large regions of hypoattenuation (arrows) in the bilateral middle cerebral artery territories, reflecting cytotoxic edema secondary to acute bilateral middle cerebral artery territorial infarctions without hemorrhagic transformation. The findings are indicative of cardioembolic phenomena (given various vascular distributions), hypoxic-ischemic injury, or ischemic vasculopathy secondary to COVID-19. **(b–d)** Sagittal maximum intensity projection **(b)** and axial head and neck CT angiographic images **(c, d)** show a long segment filling defect from the proximal cervical segment of the right ICA (arrow in **b**) to the intracranial ICA, with involvement of the right petrous (not shown) and cavernous ICA segments (arrow in **c**), indicative of right ICA thrombosis and occlusion. The right carotid terminus (white arrow in **d**) and right middle cerebral artery are completely occluded, and the M1 segment of the left middle cerebral artery is nearly completely occluded, with only a small sleeve of intravenous contrast material opacifying the artery (black arrow in **d**). Note that the loss of gray matter–white matter differentiation is more pronounced on the right (arrowheads in **d**).

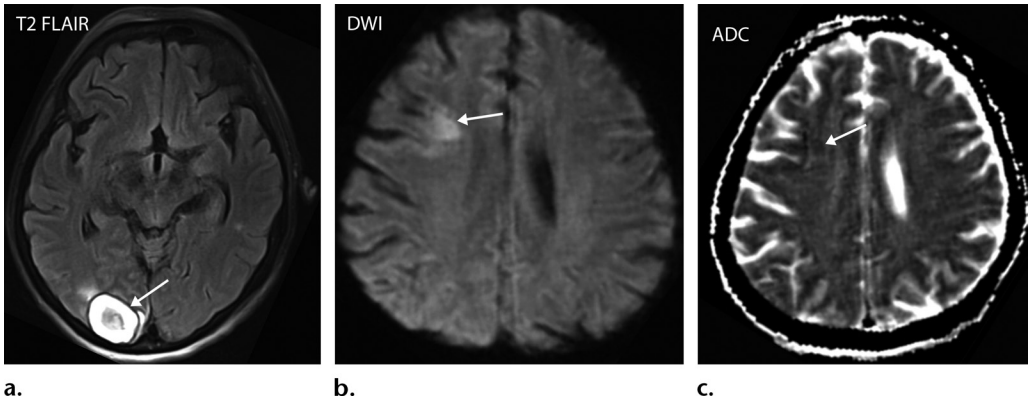

Figure 6. Multiple brain infarcts in various vascular territories and intraparenchymal hemorrhage after extubation in a 58-year-old woman with a history of diabetes mellitus who was hospitalized with COVID-19. The patient's hospital stay was complicated by multiorgan failure, line sepsis, and new neurologic deficits. **(a)** Axial T2-weighted *(T2)* FLAIR brain MR image shows a focal heterogeneous hyperintensity (arrow) within the right occipital lobe, representing an evolving intraparenchymal hematoma, with surrounding edema and mass effect. **(b, c)** Axial diffusion-weighted *(DWI)* and ADC MR images show restricted diffusion in the right frontal lobe, compatible with a small focus of acute infarct (arrow). Additional foci of restricted diffusion were depicted in the left frontal lobe (not shown), consistent with small infarcts in different vascular distributions.

hypertension. Sinus thrombosis can be visualized at nonenhanced head CT as a linear hyperattenuation within a sinus or large cortical vein and, if necessary, can be confirmed at CT venography or MR venography, at which filling defects will be depicted in the venous sinuses (Fig 8).

Venous infarcts should be suspected when they are bilateral, depicted in nonarterial ter-

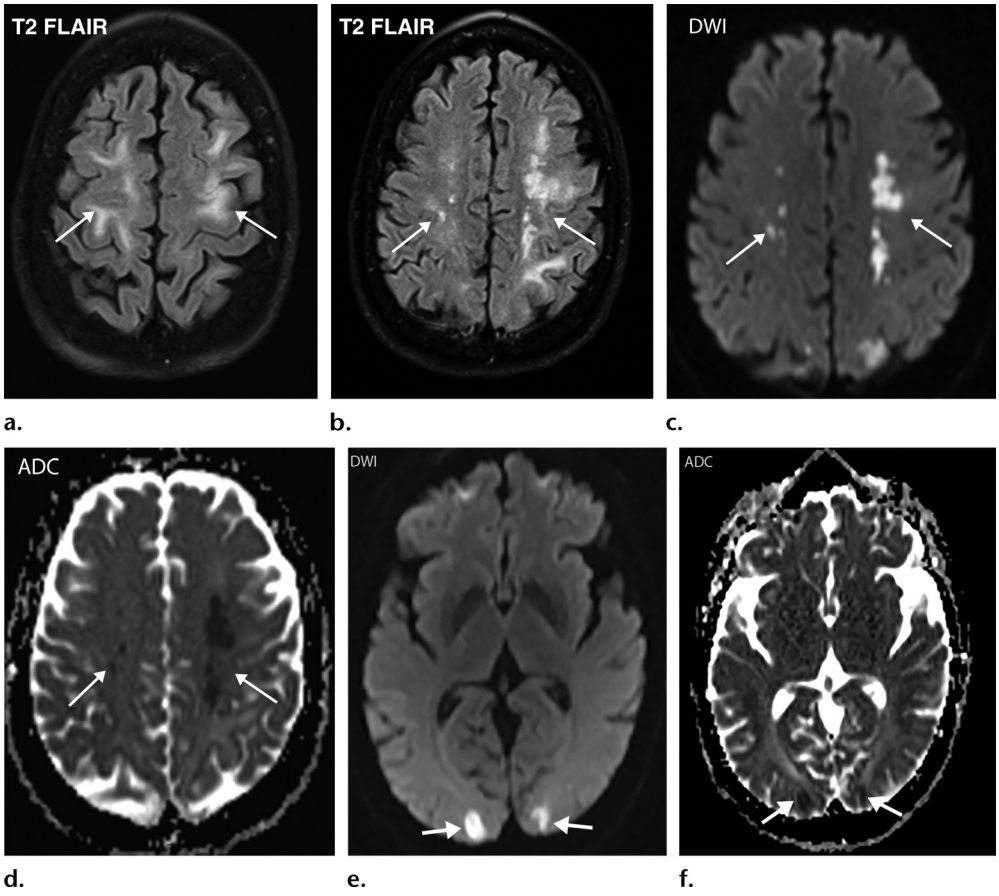

Figure 7. Watershed infarcts and cardioembolic infarcts in a 55-year-old woman with COVID-19 who presented with left gaze deviation. **(a)** Initial axial T2-weighted *(T2)* FLAIR brain MR image shows hyperintense signal abnormality (arrows), predominantly within the high frontal and parietal subcortical white matter bilaterally. **(b)** Repeat axial T2-weighted *(T2)* FLAIR MR image obtained 3 days later shows interval development of a linearly oriented pattern of signal abnormality (arrows) within the centrum semiovale bilaterally, greater on the left than on the right. **(c, d)** Axial diffusion-weighted *(DWI)* **(c)** and ADC **(d)** brain MR images show restricted diffusion in the corresponding areas of abnormality (arrows), indicative of watershed infarcts. **(e, f)** Axial diffusion-weighted *(DWI)* **(e)** and ADC **(f)** brain MR images show restricted diffusion involving the bilateral occipital lobes (arrows), indicative of additional foci of acute infarct.

ritory, and in the presence of hemorrhage (Fig 8). Hyperintense signal with T2-weighted and T2-weighted FLAIR sequences in association with restricted diffusion at diffusion-weighted imaging have been described in encephalopathy and encephalitis, especially in the inferomedial regions of the temporal lobes or insular cortex (Fig 9). Similar findings can be found with hemorrhagic diffuse leukoencephalopathy (Fig 10). Patients with COVID-19 are commonly administered anticoagulation therapy, which can become complicated by the development of spontaneous or traumatic intracranial hemorrhage (Fig 11).

Abdominal Manifestations

Although patients typically present with respiratory illness, up to 40% of patients with COVID-19 present with digestive symptoms, which include diarrhea, vomiting, and acute abdominal pain (36–38). Additionally, patients with COVID-19 commonly develop elevated liver enzymes and biliary stasis (39). The coronavirus RNA was readily detected in stool specimens of patients with SARS-CoV-2 infection, and the results of electron microscopy of biopsy and autopsy specimens confirmed active viral replication in both the small and large intestines (40–42). SARS-CoV-2 tropism to the gastrointestinal tract is likely due to its abundant expression of ACE2 receptors, specifically in the esophagus, stomach, duodenum, small and large intestine (including the rectum), and biliary endothelium (43).

US has served as a primary imaging modality for patients with abdominal and pelvic symptoms during this pandemic. Right upper quadrant and abdominal Doppler US are employed in patients with elevated liver function enzyme levels for the assessment of liver disease, gallbladder disease, biliary stasis, and portal vein thrombosis. Renal US can be performed if there is concern for renal obstruction in the setting of elevated creatinine

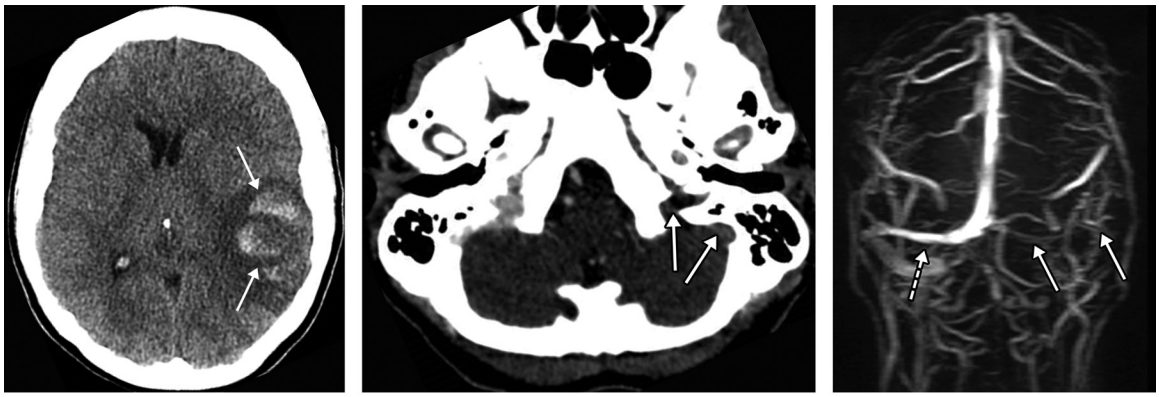

a. b. c.

Figure 8. Hemorrhagic venous infarct related to venous thrombosis in a 29-year-old woman who had two seizures after having 1 week of cough and fever and who received positive test results for COVID-19 in the emergency department. **(a)** Axial nonenhanced head CT image shows a left temporoparietal hemorrhagic venous infarct (arrows), with adjacent edema, mass effect, and minimal rightward midline shift. **(b)** Axial CT venogram shows absence of contrast material in the left sigmoid sinus (arrows), indicative of venous sinus thrombosis. **(c)** Three-dimensional maximum intensity projection image from MR venography shows thrombosis of the left transverse and sigmoid sinuses (solid arrows). Note that the right transverse sinus appears patent (dashed arrow).

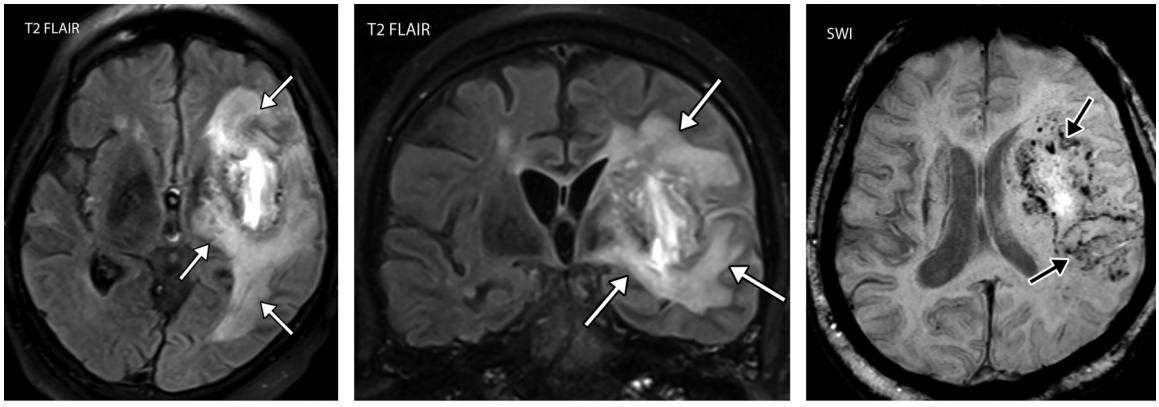

a. b. c.

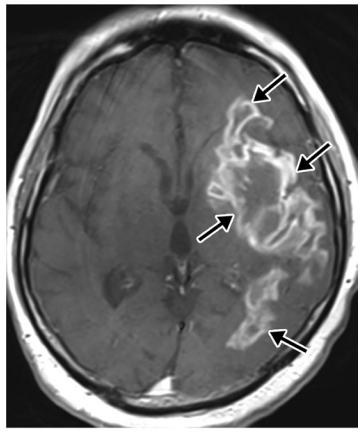

d.

Figure 9. Viral encephalitis in a 57-year-old man with a history of hypoxemic respiratory failure who required intubation in the setting of COVID-19 pneumonia. The hospital stay was complicated by hypercoagulability in the setting of COVID-19. **(a, b)** Axial **(a)** and coronal **(b)** T2-weighted *(T2)* FLAIR MR images show an infiltrative pattern of heterogeneous signal abnormality (arrows) throughout the left cerebral hemisphere involving the frontal, temporal, and occipital lobes, as well as the basal ganglia and thalamus. **(c)** Axial susceptibility-weighted image *(SWI)* shows multiple nodular and curvilinear foci of abnormal magnetic susceptibility (arrows), consistent with foci of parenchymal and subarachnoid hemorrhage. **(d)** Axial post-contrast T1-weighted MR image shows an amorphous curvilinear pattern of avid contrast enhancement (arrows).

levels and decreased urine output, and renal Doppler US may also detect renal infarction.

Doppler US can be performed in patients with suspected abdominal venous or arterial thrombosis. During the COVID-19 pandemic, there has been a significant increase in the utilization of point-of-care US by radiologists, as well as in emergency departments, medical wards, and intensive care units. In addition to evaluation of respiratory abnormalities, point-of-care US has been shown to be helpful in monitoring levels of dehydration through the assessment of the inferior vena cava, pericardial and pleural effusions, hydronephrosis, intravenous line placement, and more (44).

Multiple institutions have developed customized abbreviated US protocols in an attempt to minimize sonographer exposure to virus particles while performing US examinations in patients with COVID-19. These protocols have been

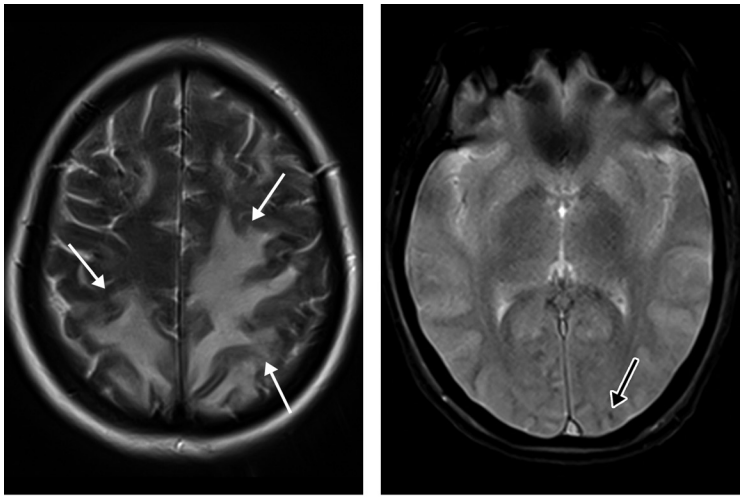

a. b.

Figure 10. Hemorrhagic diffuse leukoencephalopathy in a 43-year-old woman with COVID-19. The hospital stay was complicated by inability to follow commands and persistently depressed status after extubation. The laboratory test results showed markedly elevated D-dimer levels (>7.6 mg/mL), international normalized ratio level (1.4), and platelet count (290). **(a)** Axial T2-weighted MR image shows confluent bilateral signal hyperintensities (arrows) in the white matter of both parietal lobes. No associated diffusion restriction was depicted on diffusion-weighted or ADC images (not shown). **(b)** Axial gradient-echo MR image shows punctate microhemorrhages (arrow) in the subcortical white matter of the left occipital lobe. Multiple microhemorrhages were scattered throughout the cerebral hemispheres bilaterally and in the splenium of the corpus callosum (not shown).

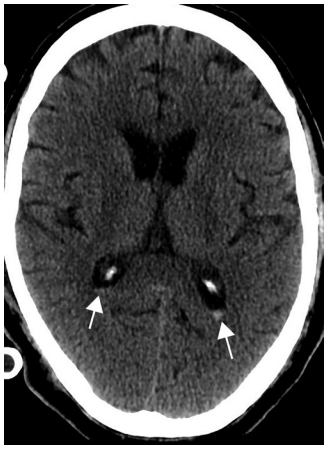

Figure 11. Intraventricular hemorrhage in a 65-year-old man receiving anticoagulation therapy in the intensive care unit as treatment for severe COVID-19 pneumonia. Axial nonenhanced CT image of the head shows a small amount of layering hyperattenuating fluid in the bilateral atria of the lateral ventricles, compatible with either spontaneous or traumatic acute intraventricular hemorrhage.

designed to focus on obtaining essential images to answer a pertinent clinical question. It has also been recommended to obtain cine clips of critical structures rather than multiple static images to minimize the time of scanning and the need for repeat examinations (45). Similarly, to decrease imaging time, some institutions have implemented postprocessing and image labeling after the examination.

Patients presenting to the emergency department with nonspecific gastrointestinal symptoms such as abdominal pain may undergo abdominopelvic CT when a COVID-19 diagnosis is not the primary consideration (46). The presence of bilateral ground-glass opacities at the lung bases should raise concern for COVID-19, and appropriate disinfectant and preventative measures should be followed for cleaning the equipment and alerting personnel. In the nonemergent setting, CT of the abdomen and pelvis with intravenous contrast material can be performed in patients with COVID-19 in whom abdominal complications such as bowel ischemia and perforation, solid organ injury or infarct, and cholestasis-related complications are suspected. Generally, CT images are obtained in the portal venous phase. However, CT angiography and venography can be performed in cases of suspected abdominal vascular thrombosis.

A recent preliminary observational study performed in 412 patients with 224 abdominal imaging examinations showed that bowel abnormalities and cholestasis were common findings at abdominal imaging (47). In this study, the most common indications for performing right upper quadrant US were elevated liver function enzyme levels and to evaluate for a source of infection. The common indications for CT were abdominal pain and to evaluate for a source of infection. Nausea, vomiting, diarrhea, and suspected bowel ischemia were less common indications (47). It is important to note that some patients with COVID-19 who initially presented with symptoms of abdominal pain did not have any detectable abdominal findings, and it is thought that their symptoms were attributable to referred pain. This is a similar phenomenon to that seen in other basilar pneumonias (particularly disease located near the pleura or diaphragm) caused by multiple organisms (eg, *Legionella*, *Mycoplasma* species) and has been reported in children as well as in adults (46).

Intestinal Manifestations

Intestinal involvement related to COVID-19 can be in the form of gastritis, enteritis, colitis, or a combination of two or all entities. They result from either direct viral infection, virus-induced bowel inflammation, or bowel wall ischemia. In patients with COVID-19, bowel wall ischemia occurs in the setting of either arterial macro- or microthrombosis or venous occlusion and mesenteric congestion and inflammation. As it was noticed with other types of coronaviruses, there have been multiple reported cases of enterocolitis and bowel ischemia in adult

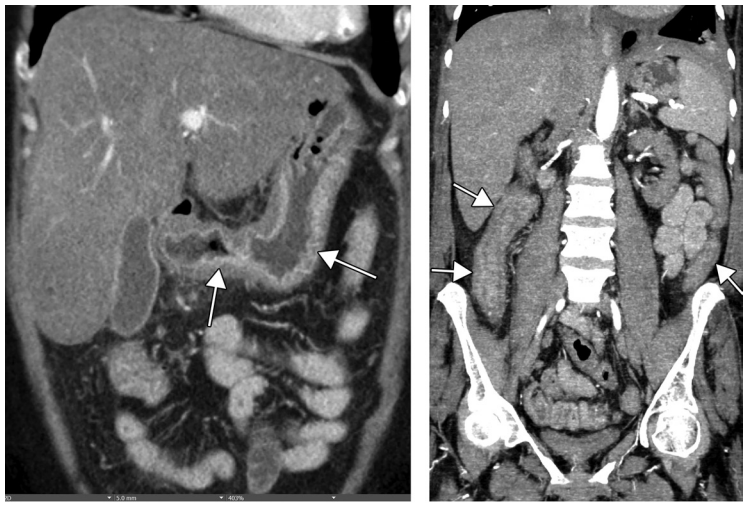

Figure 12. Gastritis and colitis in two patients who each presented with epigastric and abdominal pain and received positive test results for COVID-19 in the emergency department. Coronal contrast-enhanced CT images of the abdomen and pelvis show thickening of the gastric wall and associated mucosal hyperenhancement (arrows in **a**) and thickening of the ascending and descending colon with mucosal enhancement (arrows in **b**), findings that are indicative of gastritis **(a)** and colitis **(b)**, respectively. Note the hepatic steatosis in **a**.

a. **b.**

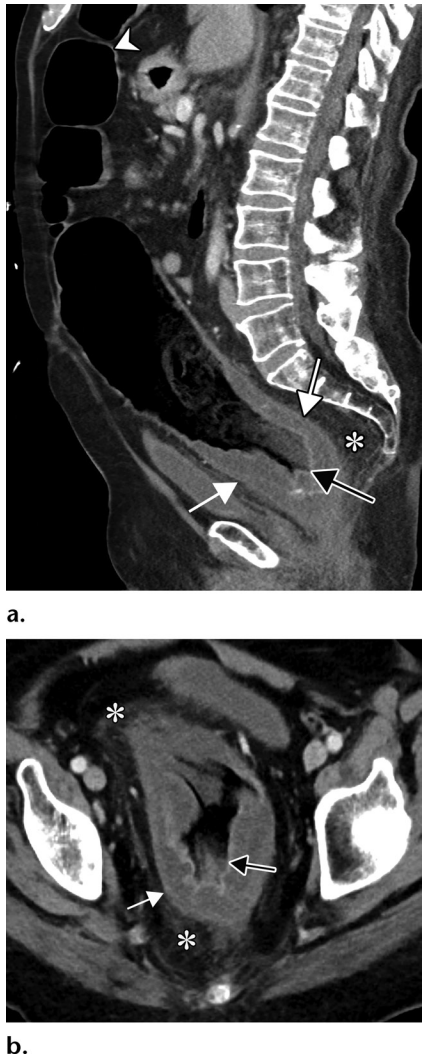

Figure 13. Proctocolitis in a 72-year-old man who presented to the emergency department with abdominal pain and fever and was diagnosed with COVID-19. Sagittal **(a)** and axial **(b)** contrast-enhanced CT images of the abdomen and pelvis show marked edema of the distended rectal wall (white arrows), with hyperenhancing mucosa (black arrow) and significant inflammatory changes in the surrounding perirectal fat (*). Note that the remaining large bowel wall is normal (arrowhead in **a**), and no significant amount of stool is depicted in the rectum. On the day of hospital admission, CT images of the abdomen and pelvis obtained through the lung bases depicted bilateral peripheral airspace opacities, ground-glass opacities, and areas of consolidations (not shown), findings typical of COVID-19 pneumonia.

a.

b.

patients with COVID-19 and hemorrhagic enterocolitis and necrotizing enterocolitis in infants with coronavirus infection (48–50).

Abdominal and pelvic CT findings of viral gastritis and/or enterocolitis that have been described in COVID-19 include wall thickening and edema (29% of patients), with predominant colorectal and small bowel involvement, fluid-filled mildly distended intestinal lumen (43% of patients), and mucosal hyperenhancement (Figs 12, 13) (47). Thickening of the bowel wall is usually attributable to submucosal edema and edema of the bowel folds, resulting in an accordion sign, similar to those findings seen in other forms of viral enteritis (51). In some cases, bowel wall thickening can resemble graft-versus-host disease at imaging, with areas of narrowing and dilatation, mucosal hyperenhancement, and ribbonlike or featureless appearance of the wall owing to bowel folds edema (Fig E2). Inflammatory changes in the surrounding fat also commonly manifest and are thought to be attributable to COVID-19–related immunoreaction and cytokine production (50,52).

Dependent on the severity and acuity of vascular compromise, COVID-19–related bowel ischemia can be divided into early, intermediate, and late presentations. The causes of bowel ischemia may not always be identified at imaging. However, taking into account that there is a strong association between COVID-19 and vascular coagulopathy, thromboembolic disease within the mesenteric vasculature is a common cause of acute mesenteric (bowel) ischemia in this patient population (5,53). A vigilant and systematic approach is needed to suspect, diagnose, and manage this otherwise fatal

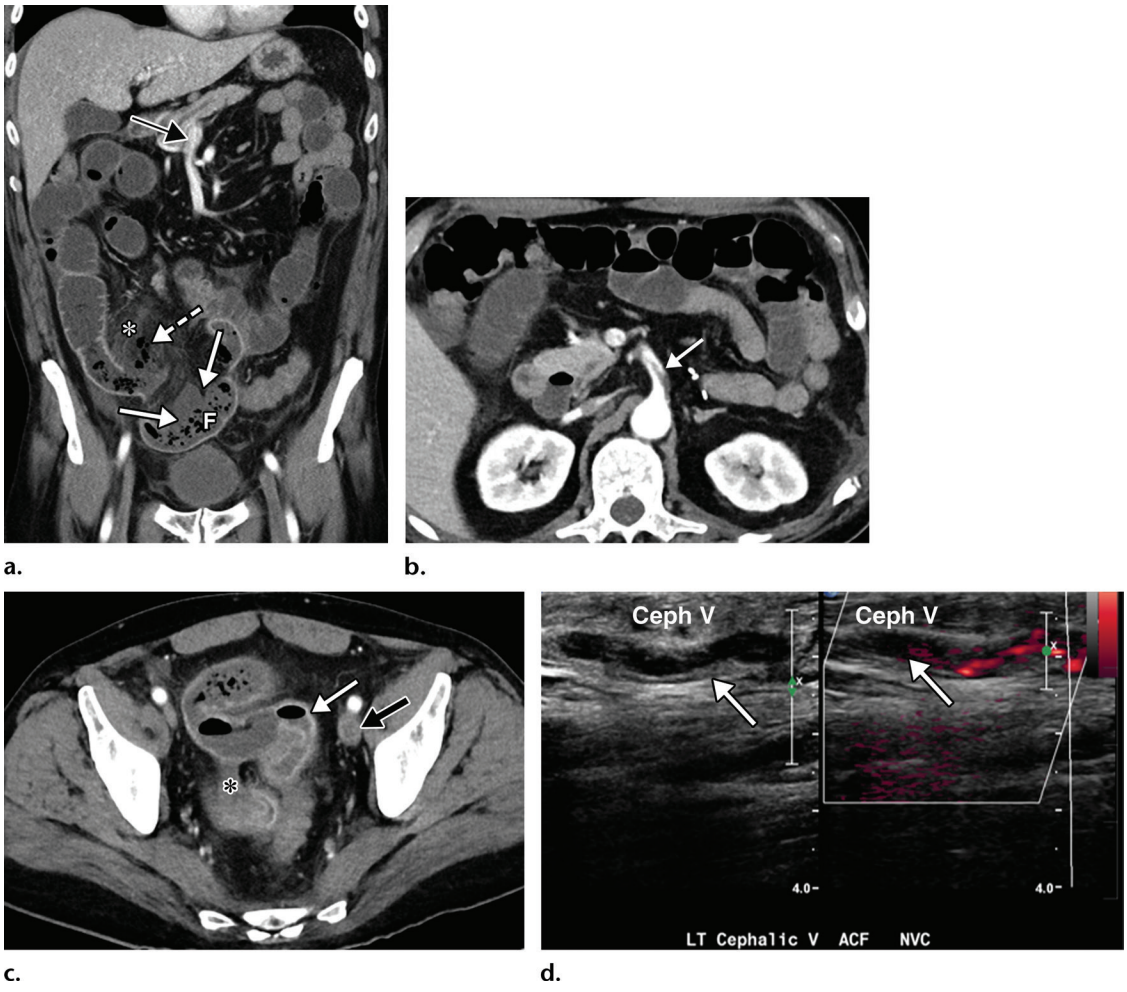

Figure 14. Superior mesenteric artery thrombosis complicated by bowel ischemia and perforation in a 54-year-old man who presented to the emergency department with abdominal pain and was diagnosed with COVID-19. **(a–c)** Coronal **(a)** and axial **(b, c)** contrast-enhanced CT images of the abdomen and pelvis show mucosal hyperenhancement involving the small bowel (*F* in **a**, white arrow in **c**), with associated mild wall thickening. There is a long segment of bowel wall hypoenhancement in the distal ileum, with a large focal wall defect (solid white arrows in **a**). Note the extension of intraluminal bowel contents, fluid, and air through the defect into the peritoneum (dashed arrow in **a**). The findings are indicative of bowel ischemia with distal ileal bowel wall perforation. There are multiple fluid-filled dilated loops of small bowel proximal to this region, suggestive of an ileus. There are associated thrombi within the proximal superior mesenteric artery (black arrow in **a**, arrow in **b**) and in the distal ileal branches (not shown). Mesenteric congestion and trace ascites are noted (∗ in **a** and **c**). However, no organized fluid collection is depicted. Note the enlarged nonenhancing left external iliac vein, compatible with deep vein thrombosis (black arrow in **c**). **(d)** Gray-scale (left) and power Doppler (right) US images of the left upper extremity, obtained owing to arm swelling, show a near-occlusive thrombus extending from the forearm to the upper humeral segment of the cephalic vein *(Ceph V)* (arrows in **d**).

complication of severe COVID-19 (53). Therefore, the mesenteric vasculature should be carefully assessed for possible arterial or venous thrombosis involving the main arterial and venous blood supply to the bowel, including the superior and inferior mesenteric arteries and veins and portal vein (Fig 14, E3).

Mesenteric thrombus can be readily visualized at CT angiography and in some cases in the portal venous phase as a filling defect in the lumen, either at the more proximal aspect of the artery, extending from the aorta, or more distally (Fig 14, E3). Thick-walled, edematous, fluid-filled, and dilated bowel (in some cases >3 cm) should raise suspicion for acute mesenteric ischemia at CT (53), and nonenhancing thickened bowel suggests bowel infarction. On CT images, the early phase of bowel ischemia may only show contracted gasless bowel that, when progressed, may transform into dilated gas-filled bowel with a paper-thin bowel wall. The CT findings of the later phase of ischemia include the development of intestinal wall pneumatosis, absence of mucosal enhancement, and luminal dilatation (Figs 14, 15, E4). Portal venous and mesenteric gas may also be apparent. Bowel infarction can result in frank bowel wall perforation, which would be visualized at imaging as discontinuity of the bowel wall, with an associated localized collection of air and/or adjacent fluid collection and/or abscess

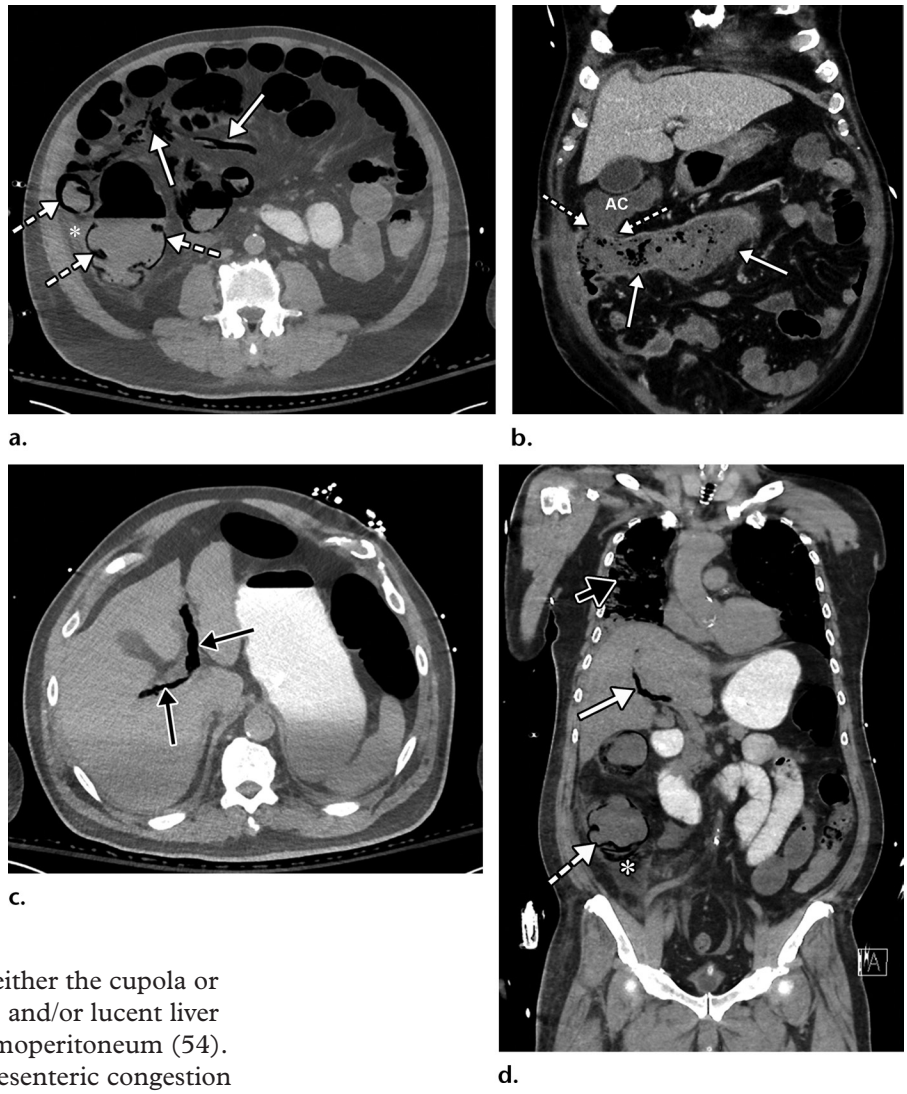

Figure 15. Bowel ischemia and perforation as a complication of COVID-19 in a 65-year-old man with a history of asthma, hypertension, and hyperlipidemia. **(a–c)** Axial (**a**, **c**) and coronal (**b**, **d**) intravenous contrast material–enhanced CT images of the abdomen and pelvis show significant pneumatosis of the cecum and right ascending colon (dashed arrows in **a** and **d**), with associated perforation of the ascending colon (*AC* and dashed arrows in **b**) and a large complex fluid collection with an enhancing rim, indicative of an abscess (solid arrows in **b**). The abscess is filled with extravasated fecal material. Note the mesenteric venous gas (solid arrows in **a**), associated with pneumatosis. Note also the small amount of ascites and mesenteric congestion (* in **a** and **d**). Portal venous gas is present (solid arrows in **c** and **d**). Peripheral airspace disease (black arrow in **d**) in the right lower lobe is also depicted.

(Figs 14, 15). Presence of either the cupola or saddlebag sign, Rigler sign, and/or lucent liver sign are indicative of pneumoperitoneum (54).

Although evidence of mesenteric congestion and hyperemia may be signs of microthrombosis, microthrombosis of the vascular beds of the pericolonic mesentery and submucosal arterioles of the bowel wall, which have been described in pathology reports from autopsy in patients who died from COVID-19, cannot usually be detected at imaging (47). Bowel infarction can be accompanied by denudation of the epithelium, which can be seen on direct visualization of the intestinal lumen (Fig 16, E4).

Hemorrhagic transformation may also be apparent at CT, characterized by the presence of hyperattenuating material within the lumen of the affected bowel. Pneumatosis and portal venous gas were identified in 20% of CT examinations performed in patients with COVID-19 in the intensive care unit (47). Pneumatosis and portal gas may also be readily detected on abdominal radiographs and US images and if found should prompt a search for the causes and location of bowel ischemia (Fig 15). However, the presence of pneumatosis must be interpreted with caution, as it may manifest secondary to mechanical ventilation in patients with severe COVID-19 or may represent an extension of air in the thorax (pneumothorax, pneumopericardium, or pneumomediastinum) (Fig 17) (53).

Abdominal Solid Organ Manifestations

Liver and Biliary Manifestations

The liver is the most frequently damaged organ outside of those of the respiratory system in COVID-19. The mechanism of hepatic injury is not fully understood, although it is most likely multifactorial and attributable to direct viral infection that results in damage to cholangiocytes, immune-related injury, and/or drug hepatotoxicity (55,56).

A substantial proportion of patients with severe acute respiratory syndrome (SARS) and patients with COVID-19 demonstrate variable degrees of liver damage (57). The ACE2 receptor has been found to be expressed in the liver, specifically in cholangiocytes (epithelial cells of the bile ducts) rather than in hepatocytes, and this may be

a. b. c.

Figure 16. Ischemic enterocolitis, periportal edema, mesenteric congestion, ascites, and multifocal bilateral native and renal transplant infarcts in a severely ill 75-year-old man with COVID-19 pneumonia, elevated liver function test results, and oliguria. **(a, b)** Coronal **(a)** and axial **(b)** contrast-enhanced images of the abdomen and pelvis show marked pericholecystic and periportal edema (white arrows) and thickened small and large bowel (black arrows). Note that the colon is fluid filled. Multifocal wedge-shaped areas of hypoattenuation are depicted in the renal cortex of the transplant kidney allograft and native kidneys (arrowheads), compatible with multifocal native renal and renal transplant infarcts. Note the marked heterogeneity of the liver parenchyma that could be attributable to hepatitis (∗ in **a**). The main mesenteric vasculature was patent. Mesenteric congestion and ascites were also present, implying the manifestation of mesenteric ischemia, likely as a result of microthrombosis. **(c)** Endoscopic image of the left colon shows denudation of the colonic epithelium, compatible with ischemic colitis. *(*Case courtesy of Christine [Cooky] Menias, MD, Mayo Clinic, Phoenix, Ariz.)

responsible for liver damage in COVID-19 (57). Researchers have found that viral infection with SARS-CoV-2 impairs the barrier and bile acid transport functions of cholangiocytes through dysregulation of genes involved in tight junction formation and bile acid transportation. This could explain the accumulation of bile acids and resultant liver damage in patients (58).

Liver injury manifests as elevation of hepatic enzyme levels. Current data show that 14.8%–53% of patients with COVID-19 have abnormal levels of alanine aminotransferase and aspartate aminotransferase during the course of disease and mild elevation in serum bilirubin levels (37,59–62). Also, approximately 50% of patients with COVID-19 had increased levels of γ-glutamyl transferase (GGT) (39). In the published literature to date, hepatic manifestations of COVID-19 were mostly mild and transient, although severe liver damage may occur. The proportion of liver injury was also higher in patients with severe COVID-19 (63). Periportal necrosis, lymphocytic infiltration of the sinusoids, dense portal infiltration by abnormally small lymphocytes, central vein thrombosis, and cirrhotic changes with thick fibrosis were all findings at liver autopsy (64,65).

Another potential cause of liver damage and elevated liver enzyme levels is microthrombosis within hepatic sinusoids, which likely is related to previously described generalized coagulopathy, as well as liver-induced coagulopathy (59). Hypoxic or ischemic hepatic injury, resulting from either a coagulopathy-induced decrease in hepatic perfusion or a respiratory-induced hypoxia, may also result in high serum aminotransferase concentrations (66).

Although US, CT, and MRI are all excellent modalities for the evaluation of hepatic and biliary disease, the imaging findings in COVID-19 may not be pathogen-specific, and findings are commonly nonspecific and subtle. At cross-sectional imaging, periportal edema and heterogeneity of the liver parenchyma should raise concern for hepatitis (Fig 16). Periportal edema may be more apparent at both CT and MRI (Fig 16). There has also been increased prevalence of hepatic steatosis in patients with COVID-19 that is likely attributable to the known association between infection and obesity (64). In fact, it has been reported that hepatic steatosis is an independent risk factor of severe disease (67).

Biliary stasis may be diagnosed by recognition of gallbladder and intrahepatic biliary ductal dilatation, without a causative obstructive mass or stone. Sludge and stones within a dilated gallbladder, reflective of cholestasis, were detected in 54% of patients with COVID-19, and it is important to note that acute cholecystitis can develop as a result of biliary stasis (Figs 18, 19) (47). In comparison, the incidence for the development of gallstones in the general population is about 10%–20% (68).

Complications related to micro- and macrothrombosis may not be readily apparent at Doppler US, contrast-enhanced CT, or MRI. Echogenic mobile foci detected at gray-scale US within the portal vein and its branches, extending to the

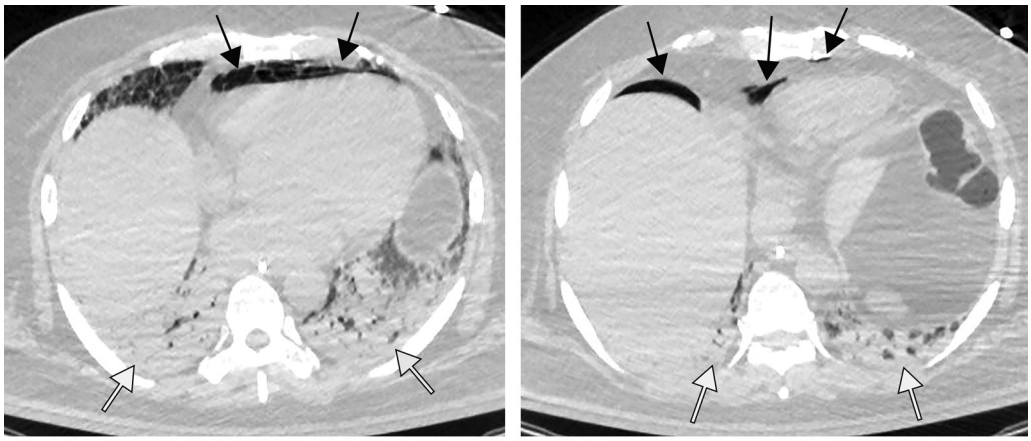

a. b.

Figure 17. Pneumopericardium with air dissecting into the peritoneum, mimicking bowel perforation, in a 64-year-old man who underwent intubation for COVID-19 pneumonia. **(a)** Axial nonenhanced chest CT image shows pneumopericardium (black arrows) and bibasilar airspace consolidations (white arrows), compatible with COVID-19 pneumonia. **(b)** Axial nonenhanced CT image of the abdomen and pelvis shows pneumopericardium and free air under the diaphragm, anterior to the liver (black arrows), without findings of bowel wall ischemia to suggest a perforation (not shown). Note the bibasilar consolidations (white arrows).

periphery of the liver, is indicative of portal venous gas, which implies the presence of bowel ischemia. Gas in the portal system can be confirmed by the visualization of specific spikes corresponding to air bubbles at spectral Doppler US interrogation of the portal vein.

As discussed previously, the bowel should be evaluated for possible evidence of bowel ischemia and/or perforation by using CT or less commonly US, and the mesenteric vasculature should be assessed for patency. Absent flow at color or spectral Doppler US in one of the hepatic vascular systems should raise suspicion for hepatic vascular thrombosis, which may affect the hepatic veins (central and/or peripheral branches), the intrahepatic inferior vena cava, and/or the portal vein (Fig E5) (69–72). It is important to note that other venous thromboses, such as those involving the renal, ovarian, or deep pelvic veins, may also be depicted (Fig 20) (73,74). Dependent on the acuity of the thrombosis, a clot may or may not be visualized at gray-scale US, and the affected vein may appear distended by the blood clot. The corresponding finding of a filling defect may be observed within the affected vessel at contrast-enhanced CT and gadolinium-enhanced MRI (Figs 20, E5).

Vascular Complications of Solid Organs

Solid organ infarcts may also be visualized at abdominal imaging in patients with COVID-19, affecting the kidney, spleen, and liver (47) (Figs 16, 18, 21–23). In a recent study of 141 patients who underwent abdominopelvic CT, 18% had solid organ infarcts (75). At Doppler US, decreased vascularity may be depicted within a solid organ, indicative of an infarct, and in these cases it is essential to assess the primary vasculature of the affected organ for the presence of a blood clot (Fig 22). Contrast-enhanced CT images may show a hypoattenuated wedge-shaped area in the solid organ parenchyma, corresponding to the infarct. Vascular thrombosis may be seen as a filling defect within one or more of the supplying vessels at CT and US (Fig E5).

Pancreas

Pancreatic injury has been described in COVID-19 and is thought to be a result of either direct or indirect mechanisms. The direct mechanism stems from a cytopathic effect mediated by local viral replication (pancreatic islet and exocrine gland cells have abundant ACE2 receptors), whereas the indirect mechanism pertains to either a systemic response to respiratory failure or a harmful immune response induced by the virus itself (76,77). Wang et al (77) found that 17% of patients with diagnosed COVID-19 had pancreatic injury. Direct injury to the islet cells can result in acute diabetes (78). Pancreatitis can either be confirmed by laboratory data (elevated lipase and amylase levels) or can be diagnosed at imaging (77). Changes within the pancreatic parenchyma, such as hypoechogenicity and heterogeneity at US or hypoattenuation and lack of enhancement at CT, with associated peri-pancreatic inflammatory changes, should raise concern for pancreatitis (Fig 24).

Urogenital Tract

Acute kidney injury is commonly encountered among critically ill patients with COVID-19, affecting approximately 20%–40% of patients ad-

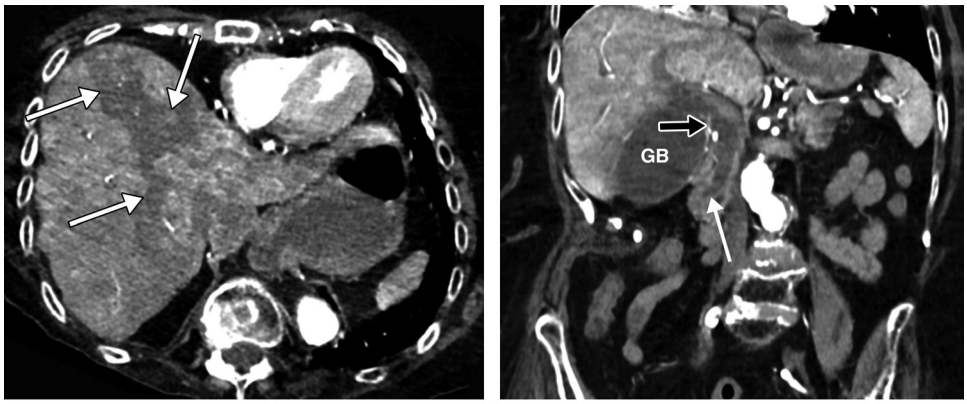

a. b.

Figure 18. Heterogeneous liver enhancement and biliary stasis in an 84-year-old woman with a history of hypertension and asthma who was admitted to the intensive care unit for hypoxic respiratory failure secondary to COVID-19 pneumonia and septic shock. The results of a laboratory test also confirmed elevated transaminase levels (aspartate transaminase, 1085 U/L; alanine transaminase, 741 U/L). The patient died 3 days later despite cholecystostomy placement. Axial **(a)** and coronal **(b)** CT angiographic images of the abdomen and pelvis show marked heterogeneous enhancement within the liver, with multiple areas of hypoenhancement along the biliary distribution (arrows in **a**). The gallbladder *(GB)* is distended, and there is a marked dilatation of the extrahepatic biliary duct (black arrow in **b**), with gradual tapering of the common bile duct within its distal segment (white arrow in **b**). No radiopaque obstructive stones or sludge were visualized. The findings are indicative of biliary stasis and an infectious or inflammatory process of the gallbladder. Note that the sensitivity of gallstone evaluation at CT is variable based on the composition of the stones.

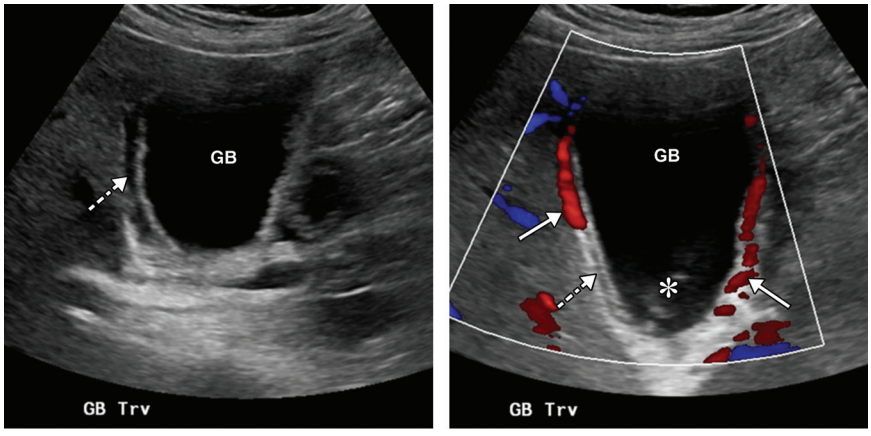

a. b.

Figure 19. Acute cholecystitis in a critically ill 64-year-old man with COVID-19 and sepsis. Gray-scale **(a)** and color Doppler **(b)** US images show a dilated gallbladder *(GB)* with sludge (∗ in **b**). Significant wall edema (dashed arrow) and hyperemia (solid arrows in **b**) are also present. The US Murphy sign was not assessed owing to the patient's altered mental status. The findings are indicative of bile stasis and acute cholecystitis. Sterile green thick dark bile was visualized during cholecystostomy placement.

mitted to the hospital and particularly to the intensive care unit in Europe and the United States (79,80). Acute kidney injury occurred at much higher rates in critically ill patients admitted to New York City hospitals, ranging from 78% to 90% (79,81–84). Approximately 20%–31% of patients admitted to the intensive care unit require renal replacement therapy (80,85,86).

There is emerging evidence of a distinct pathophysiologic mechanism of SARS-CoV-2–mediated acute kidney injury (83,87,88), which manifests clinically and pathologically by the development of acute tubular necrosis, interstitial inflammation, podocytopathy, microangiopathy, and collapsing glomerulopathy (87). US may show increased cortical echogenicity or heterogeneity and loss of corticomedullary differentiation in patients with COVID-19 and acute kidney injury. In cases of renal infarction, heterogeneity and hypoperfusion of the renal parenchyma and wedge-shaped areas of decreased perfusion and/or enhancement may be visualized at US and contrast-enhanced CT and may be multifocal, involving both kidneys (Figs 21, 22) (89). It is important to note that use of contrast material may not be possible if renal function is impaired, thus making US the first-line imaging modality of choice in the evaluation of COVID-19 in patients with suspected renal vascular insult. In addition, US contrast material can be administered to patients that cannot receive intravenous iodinated contrast material and may help demonstrate perfusion abnormalities and vascular thrombosis.

Figure 20. Ovarian vein thrombosis in a 27-year-old woman who presented to the emergency department with right flank pain. Reverse transcription–polymerase chain reaction test results confirmed COVID-19. Coronal contrast-enhanced CT image of the abdomen and pelvis shows a long segment filling defect (arrows) in the left ovarian vein, indicative of gonadal vein thrombosis. Given the positive COVID-19 results, it is uncertain if the viral infection was the cause of the thrombosis, as no other preexisting conditions or risk factors were identified.

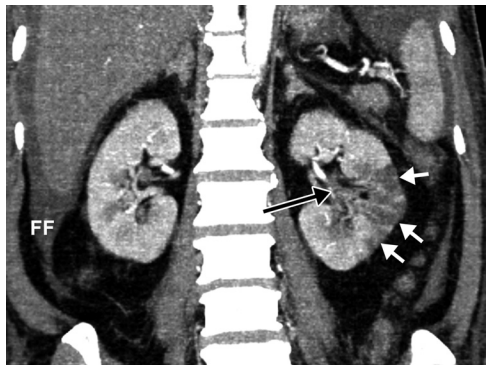

Figure 21. Renal infarcts in a 57-year-old man with COVID-19, diagnosed after presenting to the emergency department with abdominal pain. Coronal contrast-enhanced CT image of the abdomen and pelvis shows multiple linear hypoattenuating areas, extending from the left renal sinus to the surface of the cortex (white arrows). Note the occlusive thrombus (black arrow) in the segmental left renal artery. The findings are indicative of an infarct of the left kidney. Small wedge-shaped regions of hypoattenuation were also present in the right kidney, indicative of an infarct (not shown). Note the small amount of perihepatic free fluid *(FF)*.

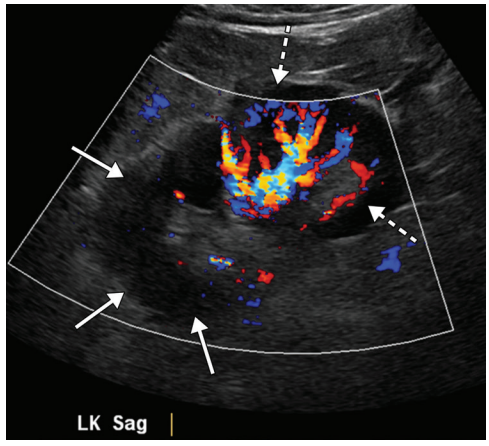

Figure 22. Renal infarct in a critically ill 52-year-old man who underwent intubation for COVID-19 and who presented with oliguria and was diagnosed with elevated creatinine levels. Sagittal color Doppler US image shows a focal area of hypoperfusion (solid arrows) in the upper pole of the left kidney, compatible with an infarct. Normal perfusion (dashed arrows) is seen in the lower pole of the kidney. Bilateral patchy ground-glass opacities, a typical finding of COVID-19 pneumonia, were depicted at chest radiography (not shown).

There is medium expression of ACE2 receptors in the urinary bladder, thus offering affinity for SARS-CoV-2 viral binding and cell entry (90). This process can result in the development of interstitial cystitis and/or hemorrhagic cystitis, which is evident at US and CT by diffuse irregularity and wall thickening of the urinary bladder (Figs 23, 25). Additionally, evidence suggests that SARS-CoV-2 infection may involve the testes by targeting epithelial cells of testicular seminiferous tubules and Leydig cells, resulting in apoptosis and immune-mediated autoimmune orchitis and gonadal dysfunction (91).

Spleen and Lymph Nodes

It has been shown that splenic injury is commonly encountered in patients with COVID-19, as SARS-CoV-2 can directly target macrophages and dendritic cells in the spleen and lymph nodes. Additionally, red pulp cells and endothelial cells of blood vessels demonstrate an abundance of ACE2 receptors on their surfaces, which allow viral particles to enter and cause direct damage (65). Splenic parenchymal congestion, hemorrhage, and a lack of lymphoid follicles were all evident at autopsy in patients who died from COVID-19, in addition to splenic parenchymal atrophy (as evidenced by the presence of fibrous tissue hyperplasia within splenic sinuses) (92). Splenic atrophy has been associated with significant lymphocytopenia, as well as macrophage proliferation and macrophage phagocytosis. Lymphocytopenia results from virally mediated lymphocyte apoptosis by activation of T and B cells within the spleen and lymph nodes. Thus, SARS-CoV-2 infection may cause impairment of the immune system by severe damage to the spleen and lymph nodes (92).

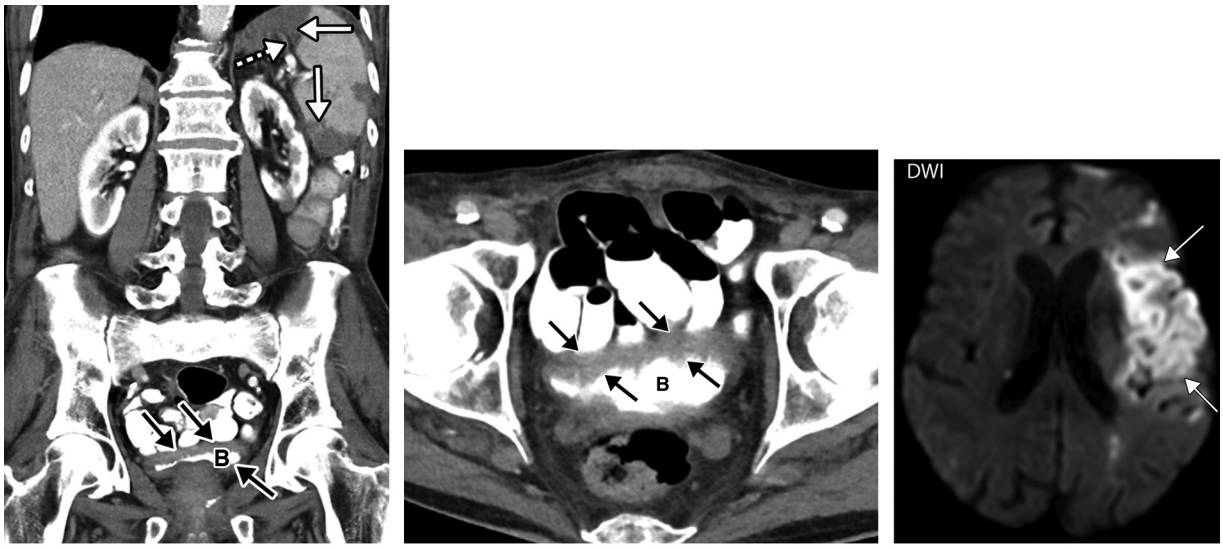

a. b. c.

Figure 23. Splenic infarcts and cystitis in an 84-year-old man with a history of newly diagnosed lung cancer who presented to the emergency department with left upper quadrant pain and urinary frequency. The test results confirmed COVID-19. **(a, b)** Coronal **(a)** and axial **(b)** contrast-enhanced CT images of the abdomen and pelvis show multiple wedge-shaped areas of hypoattenuation in the spleen (solid white arrows in **a**), indicative of multifocal splenic infarcts. Associated thrombosis of one of the splenic hilar branches supplying the anterior upper pole of the spleen is noted (dashed arrow in **a**). In addition, there is marked irregular wall thickening of the contrast material–filled urinary bladder (*B* and black arrows in **a** and **b**). It is important to note that patients with underlying conditions (such as hypercoagulable state in the setting of malignancy) are prone to develop complications of COVID-19. **(c)** Axial diffusion-weighted image *(DWI)* of the brain obtained during a hospital stay for newly developed neurological deficits shows a confluent region of restricted diffusion (arrows) within territory supplied by the left middle cerebral artery, indicative of an acute infarct. A long segment thrombus in the left middle cerebral artery was detected (not shown).

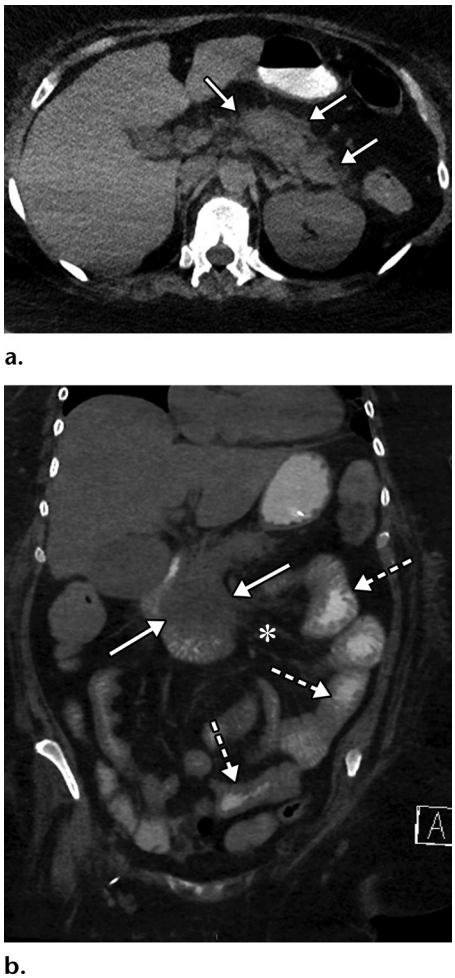

a.

b.

Figure 24. Pancreatitis and enteritis in a 56-year-old woman with COVID-19. Axial **(a)** and coronal **(b)** CT images of the abdomen and pelvis obtained with oral (no intravenous) contrast material shows a heterogeneous edematous pancreas with associated inflammatory changes and small amount of peripancreatic fluid (solid arrows), indicative of pancreatitis. Note the nondistended loops of small bowel that show mild wall thickening (dashed arrows in **b**) and mesenteric inflammation (∗ in **b**) that, although they are nonspecific in the setting of pancreatitis, may be indicative of enteritis.

To date, only a few imaging findings of splenic injuries related to COVID-19 have been reported, including splenomegaly and the development of either solitary or multifocal splenic infarcts, evidenced by wedge-shaped areas of heterogeneity and lack of splenic parenchymal perfusion (Fig 23) (93). Splenic infarct is attributable to microangiopathy or systemic hypercoagulopathy and cardiothromboembolization. The prevalence of splenic infarctions is likely underestimated, as abdominal imaging is not routinely performed owing to insufficient clinical symptoms associated with splenic infarcts, as well as general limitations of imaging in the COVID-19 population. Splenic infarcts are often diagnosed incidentally at chest CT examinations that extend to the upper abdomen (93).

Musculoskeletal Manifestations

To date, no significant musculoskeletal manifestations of COVID-19 have been reported, although a few case reports in the literature report the development of rhabdomyolysis as a potential late

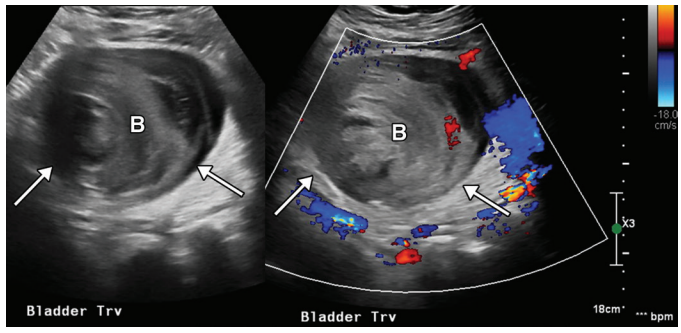

Figure 25. Urinary bladder hemorrhage in an 85-year-old man with COVID-19 pneumonia who developed hematuria and acute renal failure. Transverse gray-scale (left) and color Doppler (right) US images show a distended urinary bladder *(B)* filled with avascular heterogeneous echogenic material, indicative of urinary bladder hemorrhage (arrows).

complication of COVID-19 (94,95). Rhabdomyolysis is a life-threatening disorder that manifests with myalgia, fatigue, and pigmenturia (owing to high levels of myoglobin). Often, rhabdomyolysis is complicated by the development of acute renal failure, and the results of laboratory tests show markedly elevated levels of serum creatine kinase, with values ranging from 1500 to over 100 000 international units/L (96,97). Although mostly a clinical diagnosis, imaging findings of rhabdomyolysis include enlargement of the affected muscle or muscle group, which demonstrates heterogeneous hypoattenuation at CT (when compared with that of intact muscles) and occasional rim enhancement on postcontrast images (Fig 26).

Although not required for evaluation, MRI findings may support the diagnosis and assist in the delineation of the extent and severity of muscle injury (98). There are two types of disease recognized. Type 1 is characterized by homogeneously hyperintense signal with T2-weighted and short-τ inversion-recovery (STIR) sequences and demonstrates homogeneous enhancement following contrast material administration. Type 2 usually demonstrates heterogeneously hyperintense signal on T2-weighted images and rim enhancement following contrast material administration (99). When disease is severe, features of myonecrosis may also be present, with heterogeneous muscle parenchyma with rim enhancement and possible areas of necrosis visualized as T2-hyperintense areas when compared with the adjacent intact muscle signal intensity. The stipple sign, represented by enhancing foci within a region of otherwise nonenhanced muscle tissue surrounded by rim enhancement, is a hallmark of myonecrosis (98). Prompt clinical recognition and treatment of dehydration in COVID-19–associated rhabdomyolysis can reduce the risk of serious adverse outcomes (95).

Dermatologic and Ocular Manifestations

Dermatologic Manifestations

There are a number of known cutaneous manifestations of COVID-19, including acral areas of erythema with vesicles or pustules (pseudochilblain, similar in appearance to frostbite, also known as COVID toes) (19%), other vesicular eruptions (9%), urticarial lesions (19%), maculopapular eruptions (47%), and livedo reticularis or necrosis (6%), owing to a generalized microvascular thrombotic disorder (100). Vesicular eruptions appear early in the course of COVID-19, while the pseudochilblain pattern frequently appears late in the evolution of the disease (Fig E6) (101). The other manifestations occur in a more sporadic fashion (102). The dermatologic manifestations seem to correlate with the severity of disease, with acral lesions found in cases of less severe disease and the latter manifestations seen in more severe cases (Fig E7) (101,103).

Recognizing typical appearances of some skin manifestations (especially COVID toes) in the setting of a pending diagnosis may help radiologists and radiology staff members increase awareness that a patient undergoing imaging may have COVID-19. This would ensure proper implementation of protective practices when imaging this group, as well as increase the radiologist's awareness of other potential manifestations.

Ocular Manifestations

Several ocular manifestations of COVID-19 infection have been recognized: epiphora, conjunctival congestion, and chemosis (104). It is helpful for radiologists and radiology staff to recognize ocular manifestations of COVID-19 while performing imaging examinations, as this can increase awareness of potential COVID-19 in patients who may otherwise exhibit few or no symptoms.

Pediatric Manifestations

In the United States and globally, there have been fewer cases of COVID-19 reported in children (ages 0–17) than in adults (105). Taking into account that children comprise 22% of the U.S. population, as of August 3, 2020, data have shown that 7.3% of all cases of COVID-19 reported to the Centers for Disease Control and Prevention were in children (36,106). However, between

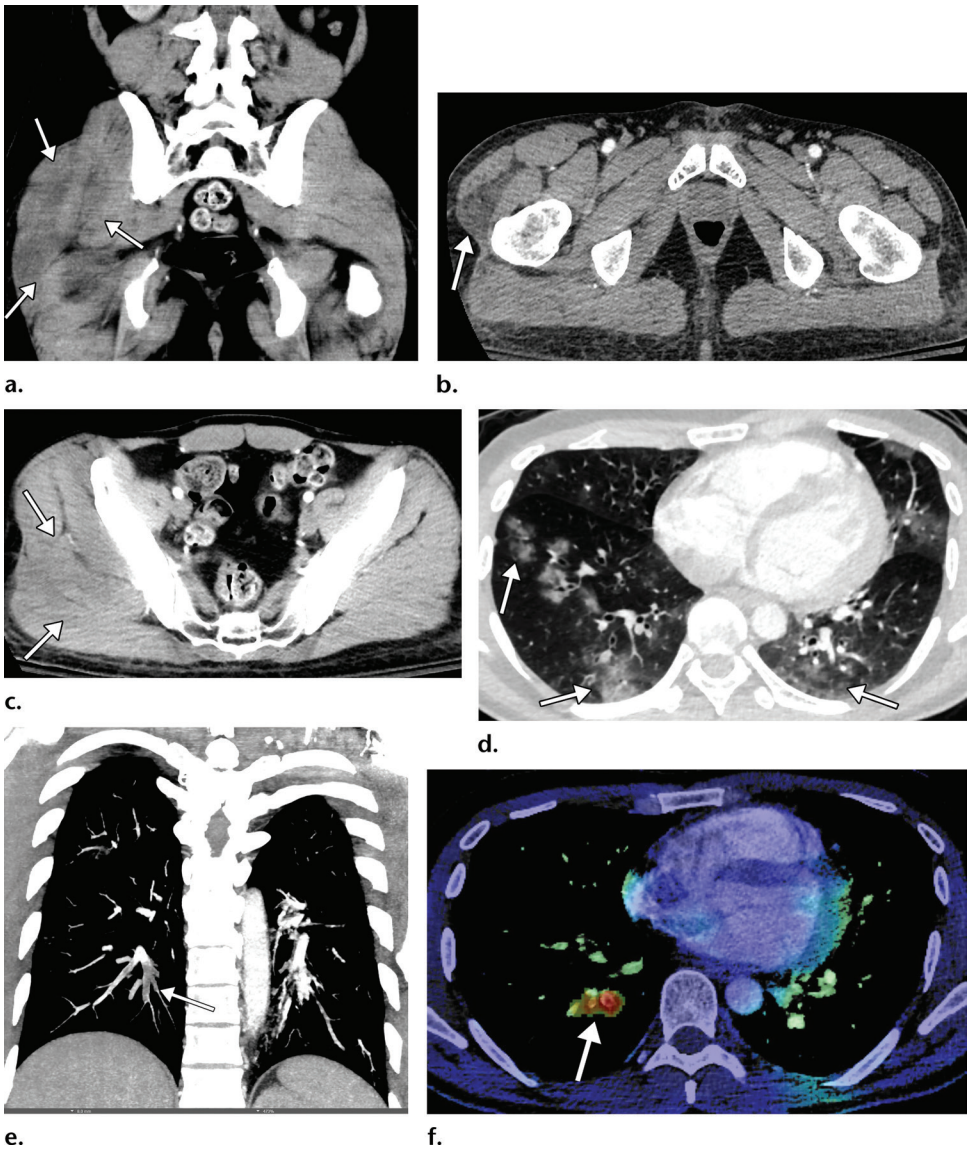

Figure 26. Rhabdomyolysis in a 34-year-old man who presented with minor trauma and was diagnosed with COVID-19 in the emergency department. Laboratory analysis results demonstrated an extremely high creatine kinase level of 35 145 U/L (normal range, 39–308 U/L). **(a–c)** Coronal **(a)** and axial **(b, c)** contrast-enhanced CT images of the pelvis show an enlarged right gluteal region (arrows) without associated fracture. **(d–f)** Axial **(d)** and coronal **(e)** contrast-enhanced chest CT images and a CT image with an artificial intelligence deep learning algorithm for the detection of pulmonary embolism **(f)** show bilateral multifocal multilobar peribronchovascular patchy airspace and ground-glass opacities (arrows in **d**), which are a typical finding for COVID-19. Multiple segmental and subsegmental right lower lobe pulmonary emboli (arrows in **e** and **f**) were also detected.

March 2020 and July 2020, there has been a steady increase in the number and rate of COVID-19 cases in children in the United States, and it is also important to note that the true incidence of SARS-CoV-2 infection in children remains unknown owing to testing-related selection bias (lack of widespread testing and the prioritization of testing for adults and those with severe illness). Data regarding the epidemiologic characteristics, transmission rates, and clinical features of pediatric infections remain limited (36,59).

According to data derived from a number of hospitalization rates in children, pediatric COVID-19 cases have relatively milder symptoms and less severe illness in general when compared with those of older patients (107). The reason for this difference between children and adults remains elusive, although there are reports that suggest that children may have lower viral loads (108). Most children who required intensive care support had preexisting conditions (36), and in the United States, infants accounted for the highest percentage of hospitalizations (15%–62%). Whereas 18.5% of adults with COVID-19 had severe disease, only 6% of children with COVID-19 exhibited severe symptoms (109).

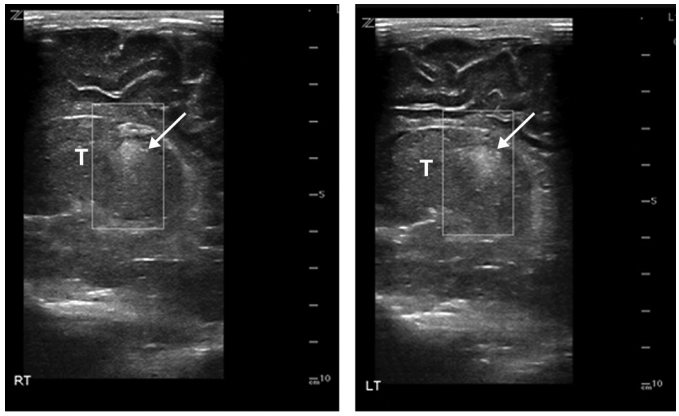

a. b.

Figure 27. Hypoxic ischemic encephalopathy in a 2-day-old full-term newborn boy who was born by cesarean delivery in a 32-year-old woman with COVID-19. Coagulopathy was diagnosed at birth, with an elevated international normalized ratio of 2.0. The infant died on day 2 following birth. Sagittal gray-scale US images of the neonatal brain obtained at the level of the right **(a)** and left **(b)** thalami *(T)* show increased echogenicity within the thalami (arrows), compatible with hypoxic ischemic encephalopathy. The adjacent midline structures are intact, and no germinal matrix or intraventricular hemorrhage was visualized. The lateral ventricles were normal in size. No parenchymal mass, hematoma, or extra-axial fluid collections were depicted.

Evidence suggests that as many as 45% of pediatric patients are asymptomatic (110), although when symptomatic, the most common manifestations are fever (95%) and cough (86%) (111). A recent multicenter multinational cohort study in Europe reported that up to 54% of symptomatic children and adolescents present with symptoms of upper respiratory tract infection, such as pharyngitis, tonsillitis, otitis media, or sinusitis (112).

Despite the tendency toward favorable outcomes in the pediatric population, a number of pediatric COVID-19 deaths have been reported in the United States and in other countries (111). Immunocompromised children and those with respiratory and/or cardiac disease comprise the largest subsets of underlying medical conditions in children with COVID-19. Coinfections are observed in 5.6% of children (111), and the mean age of presentation in the pediatric population is 8.9 years. Over three-fourths of patients (75.6%) had a history of exposure to a family member who had been diagnosed with COVID-19 or had been residing in an area with a high population of cases, both of which serve as the most common vectors for childhood infection (111).

Although chest radiography is frequently the first imaging study performed in a pediatric patient presenting with fever, cough, and/or shortness of breath, current literature describing COVID-19 findings on chest radiographs in children is relatively scarce. In a systematic review article published in *Lancet*, Hoang et al (111) reported that most patients had normal chest radiographs. At CT, diffuse bilateral ground-glass opacities were the most common finding at all stages of disease (36,113), and a peripheral distribution of pulmonary opacities was observed, similar to in adult patients. However, it is interesting to note that consolidations with a surrounding halo sign were more commonly visualized in children than adults (113), and that no associated lymphadenopathy or pleural effusions were observed (113). According to the American College of Radiology Appropriateness Criteria, imaging is not indicated in a well-appearing immunocompetent child older than 3 months of age who does not require hospitalization. However, if the child is not responding to outpatient management or requires hospitalization, chest radiography is considered the most appropriate first step in imaging evaluation (114). Similar to the adult population, the Radiological Society of North America consensus statement on pediatric patients with respect to use of CT states that chest CT should be reserved for symptomatic hospitalized patients with specific clinical indications (115). Given its relative safety and repeatability, lung US is another imaging modality that has been widely used in pediatric patients with COVID-19, with similar findings in the lungs with those in the adult population (5).

There are limited data regarding the neurologic manifestations of COVID-19 in children. At our institutions, there was a single case of a thalamic hemorrhage diagnosed in an infant who was born to a COVID-19–positive mother. Intracranial US demonstrated a geographic area of increased echogenicity in the cerebral parenchyma at the level of bilateral thalami (Fig 27). If necessary, contrast-enhanced CT of the neck can be performed in patients presenting with upper respiratory symptoms, including those of tonsillitis, otitis, and sinusitis, to evaluate for potential complications such as abscess formation (Fig 28).

In late April 2020, the National Health Service in the United Kingdom issued an alert to pediatricians about an unprecedented cluster of children who presented with symptoms of hyperinflammatory shock, with features similar to those of atypical Kawasaki disease, Kawasaki disease shock syndrome, or toxic shock syndrome. All children either received positive test results for COVID-19, had antibodies to the infection,

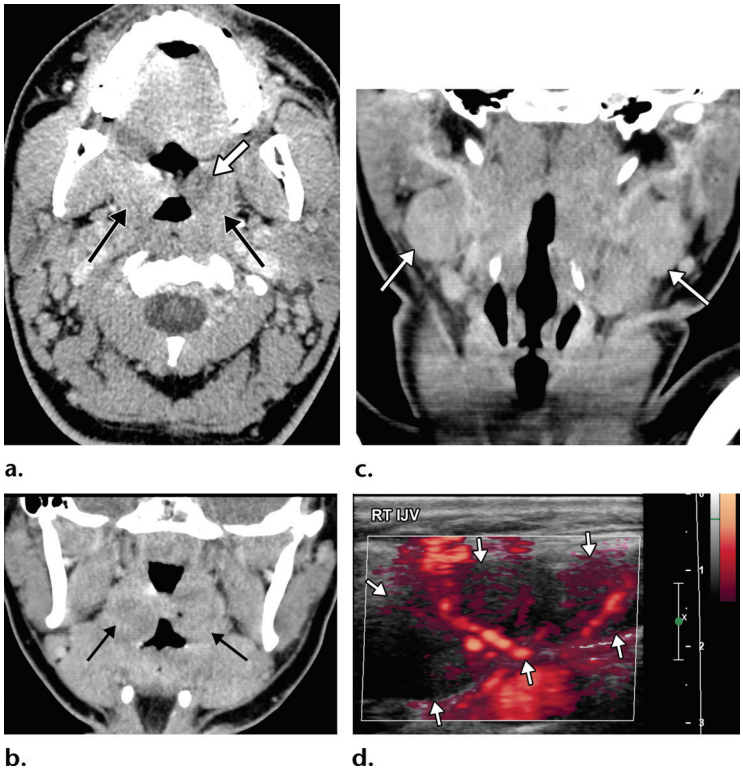

Figure 28. Tonsillitis in a 15-year-old boy who presented to the emergency department with fever, sore throat, malaise, and right neck swelling and was diagnosed with elevated D-dimer levels and inflammatory marker levels. The test results were positive for COVID-19. **(a–c)** Axial **(a)** and coronal **(b, c)** contrast-enhanced neck CT images show enlarged palatine tonsils (black arrows in **a** and arrows in **b**). A subtle ill-defined asymmetric area of hypoattenuation is depicted within the enlarged left palatine tonsil, consistent with phlegmon or early abscess (white arrow in **a**). Associated cervical lymphadenopathy (arrows in **c**) is depicted. **(d)** Sagittal power Doppler US image of the right superior neck shows a near-complete occlusive thrombus (arrows) in the right jugular vein *(RT IJV)*.

or had been exposed to patients with COVID-19 (116). Similar case reports also emerged throughout Europe and the United States, specifically in New York.

Clinical presentation included fever (38°–40°C), variable rash, conjunctivitis, peripheral edema, generalized extremity pain, and significant gastrointestinal symptoms (117–119). This presentation is currently termed pediatric multisystem inflammatory syndrome (PMIS) (116,120–122) and is thought to be caused by an autoimmune-mediated systemic response of autoantibodies to the virus. The SARS-CoV-2 antibody itself is likely responsible for provoking the immune response (116). Children who exhibit symptoms of PMIS may present with abdominal pain, vomiting, and diarrhea, and a proportion may present with acute heart failure and features of acute myocarditis (122).

Based on a recently published case series of 35 children who developed post–COVID-19 PMIS, a pattern of imaging abnormalities was described and included airway inflammation, rapidly progressive pulmonary edema, coronary artery aneurysms, and extensive abdominal inflammatory changes within the right iliac fossa, with lymphadenopathy and bowel wall thickening (119). In this series, 46% of chest radiographs were normal, and the findings on abnormal chest radiographs consisted of peribronchial cuffing and perihilar interstitial thickening (34%), which rapidly progressed to perihilar airspace opacification. Bilateral pleural effusions were seen in 14% of patients, and atelectasis (predominately involving the left lower lobe) was found in 20% of patients. Additionally, in this case series, 30%–40% patients who underwent chest CT had predominately bibasilar consolidations, with lung collapse and pleural effusions. Diffuse bilateral ground-glass opacification in combination with patchy dense consolidation was only seen in 9% (119).

In patients with PMIS, signs of cardiac dysfunction were seen in 51% of children, with abnormal echocardiographic findings depicting deteriorating myocardial function, myocarditis, pancarditis, dilated cardiomyopathy, pericardial effusions, and coronary artery aneurysms. Coronary artery aneurysms were best detected either at echocardiography or cardiac CT, with abnormalities ranging from mild single artery dilatation to large aneurysms affecting more than one coronary artery, with sizes ranging from 4 to 7.7 mm in diameter (119) (Fig 29, Movies 2,3). Myocarditis-related imaging findings are discussed in the previous cardiac section.

In children with PMIS, a wide spectrum of abdominal abnormalities can manifest that can be detected at both abdominal US and CT, with periportal and pericholecystic edema, gallbladder wall and bowel wall thickening and dilatation, splenic infarcts, hepatosplenomegaly, right lower quadrant mesenteric lymphadenopathy, and free fluid in the pelvis being among the most commonly encountered abnormalities (119). It is important to note

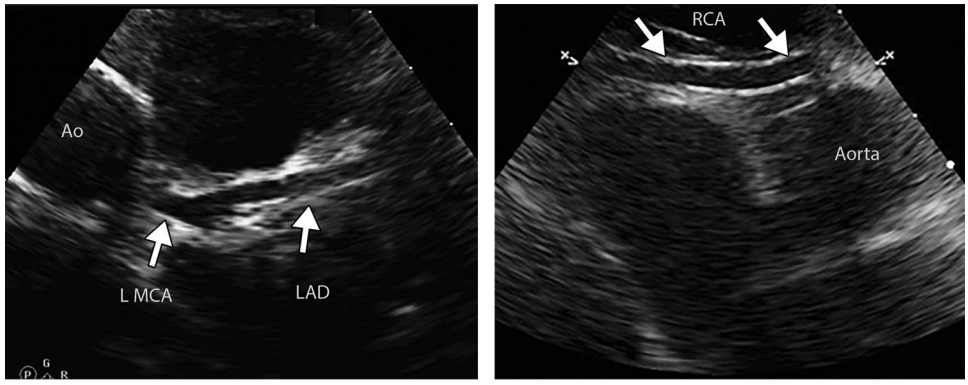

a. b.

Figure 29. Coronary artery dilatation and decreased ventricular ejection fraction in a 9-year-old boy with a recent history of COVID-19 who presented with new onset of hypotension, kidney disease, and elevated troponin and D-dimer levels (same patient as in Movies 2 and 3). Parasternal short-axis echocardiograms show lack of tapering in the left anterior descending *(LAD)* coronary artery (arrows in **a**) and the right coronary artery *(RCA)* (arrows in **b**). Left ventricular ejection fraction was decreased (not shown). *Ao* = aorta, *L MCA* = left main coronary artery. (Case courtesy of Misra Nilanjana, MD, Northwell Health, New Hyde Park, NY.)

that, on the basis of the scarcity of reported data on PMIS, caution must be taken when generalizing the results of a few reported studies to an entire population.

COVID-19 in Pregnancy

It is not currently known if pregnant patients have a higher risk of contracting COVID-19 when compared with the general population or whether they are more likely to have serious complications as a result of COVID-19 (123,124). Based on available information, it appears that pregnant patients have the same risk of contracting the infection as adults of similar age who are not pregnant. However, it is hypothesized that, owing to alterations in physiology associated with pregnancy, these patients may have an increased risk of infections in general.

In addition, a case-controlled study performed in 2014 in pregnant patients with SARS-CoV infection demonstrated that, when infected, pregnant women have a higher risk of developing severe illness (125). However, a recent study of 43 pregnant women showed that disease severity in this small cohort appeared to be similar (86% mild, 9.3% severe, and 4.7% critical) to that described in the literature in nonpregnant patients (126). It was also found that pregnancy and delivery did not aggravate the severity of COVID-19 pneumonia (127). Pregnancy complicated by ARDS that resulted in preterm delivery of a fetus has also been described (128). It has therefore been advised that pregnant women avoid exposure to the virus and practice self-hygiene and social distancing. It is important to note that the effects of the virus early in pregnancy are unknown, as no known live infants have been delivered by women infected in the first and second trimesters of pregnancy at this time.

Mother-to-fetus (vertical) transmission of coronavirus during pregnancy is currently a controversial topic. Breslin et al (126) and Chen et al (129) reported that there was no evidence for intrauterine infection caused by vertical transmission in women who develop COVID-19 pneumonia late in pregnancy. On the contrary, Pentfield et al (130) found the presence of viral RNA by the results of reverse transcription–polymerase chain reaction tests of placental membranes at the time of delivery, which suggests the need for further research into the possibility of vertical transmission. There is also a case report that describes second-trimester pregnancy resulting in miscarriage owing to COVID-19 (131). In this study, the maternal portion of the placenta tested positive for virus particles.

After birth, a newborn may be susceptible to person-to-person transmission of COVID-19. In the current literature, a small number of newborn infants have tested positive for the virus. However, it is unknown if the infants contracted the virus before or after birth. In a limited number of studies published to date, COVID-19 virus has not been detected in amniotic fluid, cord blood, neonatal throat swab specimens, or breast milk (129). Although preliminary data suggest that children are much less affected by COVID-19 than their adult counterparts, the level of risk to newborns is largely unknown (132).

Pregnant patients with COVID-19 with mild and moderate respiratory symptoms who undergo chest radiography and chest CT show typical findings of pulmonary disease, character-

ized by multifocal patchy bilateral ground-glass opacities, with crazy-paving patterns and consolidations found with disease progression. Lymphadenopathy and pleural effusions are rarely depicted (127,129,133). ARDS-related imaging findings have also been readily detected (128). Pulmonary CT angiography should be performed in pregnant patients with suspected pulmonary embolism. It is important to note that while performing CT in pregnant patients, it is preferable to use a low-radiation-dose imaging mode to decrease the risk of maternal and fetal radiation exposure, and whenever possible the abdomen and pelvis should be covered by a lead blanket. In general, US is the preferred modality for the evaluation of a pregnant patient and the fetus, as it can be used for evaluation and surveillance of the maternal lungs, assessment of potential maternal abdominal and vascular complications, and evaluation of fetal well-being, as well as the gravid uterus.

Conclusion

SARS-CoV-2 is a novel coronavirus that has rapidly resulted in a worldwide pandemic and has been the cause of extreme morbidity and mortality. It primarily affects the respiratory system but has also been shown to impact other systems in the human body, resulting in multiorgan injury and, in some cases, failure. Imaging plays a significant role in the detection, diagnosis, and assessment of virus-induced injury and associated complications. Recognizing and understanding the pathophysiology of the virus and its effects on the immune system and coagulation is paramount toward improving radiologists' ability to accurately identify key imaging findings and promptly recognize possible complications, thus minimizing the number of diagnostic misinterpretations. Owing to the complexity of viral pathophysiology and its targeting of multiple organ systems, the recognition of one complication should prompt intense scrutiny for others, particularly if patients are critically ill. A thorough knowledge of diagnostic imaging hallmarks, atypical imaging features, multisystem manifestations, and evolution of imaging findings is essential to optimize patient care.

Acknowledgments.—The authors thank Christine O. (Cooky) Menias, MD, Mayo Clinic, Ariz, for her valuable guidance and recommendations; Misra Nilanjana, MD, Northwell Health, and Henry Douglas for their help with images; and Alexandria Brackett for the assistance with literature searches and references.

References

1. Cantwell R, Clutton-Brock T, Cooper G, et al. Saving Mothers' Lives: Reviewing maternal deaths to make motherhood safer: 2006-2008—The Eighth Report of the Confidential Enquiries into Maternal Deaths in the United Kingdom. BJOG 2011;118(suppl 1):1–203 [Published correction appears in BJOG 2015;122(5):e1.].
2. COVID-19 Coronavirus Pandemic. https://www.worldometers.info/coronavirus/. Accessed August 15, 2020.
3. Wang T, Du Z, Zhu F, et al. Comorbidities and multiorgan injuries in the treatment of COVID-19. Lancet 2020;395(10228):e52.
4. Gupta A, Madhavan MV, Sehgal K, et al. Extrapulmonary manifestations of COVID-19. Nat Med 2020;26(7):1017–1032.
5. Revzin MV, Raza S, Warshawsky R, et al. Multisystem Imaging Manifestations of COVID-19, Part 1: Viral Pathogenesis and Pulmonary and Vascular System Complications. RadioGraphics 2020;40(6):1574–1599.
6. Shi S, Qin M, Shen B, et al. Association of Cardiac Injury With Mortality in Hospitalized Patients With COVID-19 in Wuhan, China. JAMA Cardiol 2020;5(7):802–810.
7. Ruan Q, Yang K, Wang W, Jiang L, Song J. Clinical predictors of mortality due to COVID-19 based on an analysis of data of 150 patients from Wuhan, China. Intensive Care Med 2020;46(5):846–848 [Published correction appears in Intensive Care Med 2020;46(6):1294–1297.].
8. Kang Y, Chen T, Mui D, et al. Cardiovascular manifestations and treatment considerations in COVID-19. Heart 2020;106(15):1132–1141.
9. Guo T, Fan Y, Chen M, et al. Cardiovascular Implications of Fatal Outcomes of Patients With Coronavirus Disease 2019 (COVID-19). JAMA Cardiol 2020;5(7):811–818.
10. Ruan Q, Yang K, Wang W, Jiang L, Song J. Correction to: Clinical predictors of mortality due to COVID-19 based on an analysis of data of 150 patients from Wuhan, China. Intensive Care Med 2020;46(6):1294–1297.
11. Puntmann VO, Carerj ML, Wieters I, et al. Outcomes of Cardiovascular Magnetic Resonance Imaging in Patients Recently Recovered From Coronavirus Disease 2019 (COVID-19). JAMA Cardiol 2020 doi: 10.1001/jamacardio.2020.3557. Published online July 27, 2020. Accessed August 15, 2020.
12. Kim IC, Kim JY, Kim HA, Han S. COVID-19-related myocarditis in a 21-year-old female patient. Eur Heart J 2020;41(19):1859.
13. Inciardi RM, Lupi L, Zaccone G, et al. Cardiac Involvement in a Patient With Coronavirus Disease 2019 (COVID-19). JAMA Cardiol 2020;5(7):819–824.
14. Sala S, Peretto G, Gramegna M, et al. Acute myocarditis presenting as a reverse Tako-Tsubo syndrome in a patient with SARS-CoV-2 respiratory infection. Eur Heart J 2020;41(19):1861–1862.
15. Arentz M, Yim E, Klaff L, et al. Characteristics and Outcomes of 21 Critically Ill Patients With COVID-19 in Washington State. JAMA 2020;323(16):1612–1614.
16. Khalil H, Alzahrani T. Cardiomyopathy Imaging. Treasure Island, Fla: StatPearls, 2020.
17. Onder G, Rezza G, Brusaferro S. Case-Fatality Rate and Characteristics of Patients Dying in Relation to COVID-19 in Italy. JAMA 2020;323(18):1775–1776.
18. Mao L, Jin H, Wang M, et al. Neurologic Manifestations of Hospitalized Patients With Coronavirus Disease 2019 in Wuhan, China. JAMA Neurol 2020;77(6):683–690.
19. Wu Y, Xu X, Chen Z, et al. Nervous system involvement after infection with COVID-19 and other coronaviruses. Brain Behav Immun 2020;87:18–22.
20. Steardo L, Steardo L Jr, Zorec R, Verkhratsky A. Neuroinfection may contribute to pathophysiology and clinical manifestations of COVID-19. Acta Physiol (Oxf) 2020;229(3):e13473.
21. Mehta P, McAuley DF, Brown M, et al. COVID-19: consider cytokine storm syndromes and immunosuppression. Lancet 2020;395(10229):1033–1034.
22. Morfopoulou S, Brown JR, Davies EG, et al. Human Coronavirus OC43 Associated with Fatal Encephalitis. N Engl J Med 2016;375(5):497–498.
23. Tsai LK, Hsieh ST, Chang YC. Neurological manifestations in severe acute respiratory syndrome. Acta Neurol Taiwan 2005;14(3):113–119.
24. Kandemirli SG, Dogan L, Sarikaya ZT, et al. Brain MRI Findings in Patients in the Intensive Care Unit with COVID-19 Infection. Radiology 2020;297(1):E232–E235.

25. Egbert AR, Cankurtaran S, Karpiak S. Brain abnormalities in COVID-19 acute/subacute phase: A rapid systematic review. Brain Behav Immun doi: 10.1016/j.bbi.2020.07.014. Published online July 17, 2020. Accessed August 15, 2020.
26. Kremer S, Lersy F, Anheim M, et al. Neurologic and neuroimaging findings in patients with COVID-19: A retrospective multicenter study. Neurology 2020;95(13):e1868–e1882.
27. Jain R, Young M, Dogra S, et al. COVID-19 related neuroimaging findings: A signal of thromboembolic complications and a strong prognostic marker of poor patient outcome. J Neurol Sci 2020;414:116923.
28. Kremer S, Lersy F, de Sèze J, et al. Brain MRI Findings in Severe COVID-19: A Retrospective Observational Study. Radiology doi: 10.1148/radiol.2020202222. Published online June 16, 2020. Accessed July 20, 2020.
29. Parsons T, Banks S, Bae C, Gelber J, Alahmadi H, Tichauer M. COVID-19-associated acute disseminated encephalomyelitis (ADEM). J Neurol 2020;267(10):2799–2802.
30. Radmanesh A, Derman A, Lui YW, et al. COVID-19-associated Diffuse Leukoencephalopathy and Microhemorrhages. Radiology 2020;297(1):E223–E227.
31. Kishfy L, Casasola M, Banankhah P, et al. Posterior reversible encephalopathy syndrome (PRES) as a neurological association in severe Covid-19. J Neurol Sci 2020;414:116943.
32. Poyiadji N, Shahin G, Noujaim D, Stone M, Patel S, Griffith B. COVID-19-associated Acute Hemorrhagic Necrotizing Encephalopathy: Imaging Features. Radiology 2020;296(2):E119–E120.
33. Morris M, Zohrabian VM. Neuroradiologists, Be Mindful of the Neuroinvasive Potential of COVID-19. AJNR Am J Neuroradiol 2020;41(6):E37–E39.
34. Vaira LA, Salzano G, Fois AG, Piombino P, De Riu G. Potential pathogenesis of ageusia and anosmia in COVID-19 patients. Int Forum Allergy Rhinol 2020;10(9):1103–1104.
35. Avula A, Nalleballe K, Narula N, et al. COVID-19 presenting as stroke. Brain Behav Immun 2020;87:115–119.
36. Wu Z, McGoogan JM. Characteristics of and Important Lessons From the Coronavirus Disease 2019 (COVID-19) Outbreak in China: Summary of a Report of 72 314 Cases From the Chinese Center for Disease Control and Prevention. JAMA 2020;323(13):1239–1242.
37. Huang C, Wang Y, Li X, et al. Clinical features of patients infected with 2019 novel coronavirus in Wuhan, China. Lancet 2020;395(10223):497–506 [Published correction appears in Lancet 2020;395(10223):496.].
38. Han W, Quan B, Guo Y, et al. The course of clinical diagnosis and treatment of a case infected with coronavirus disease 2019. J Med Virol 2020;92(5):461–463.
39. Zhang C, Shi L, Wang FS. Liver injury in COVID-19: management and challenges. Lancet Gastroenterol Hepatol 2020;5(5):428–430.
40. Hung IF, Lau SK, Woo PC, Yuen KY. Viral loads in clinical specimens and SARS manifestations. Hong Kong Med J 2009;15(Suppl 9):20–22.
41. Hoffmann M, Kleine-Weber H, Schroeder S, et al. SARS-CoV-2 Cell Entry Depends on ACE2 and TMPRSS2 and Is Blocked by a Clinically Proven Protease Inhibitor. Cell 2020;181(2):271–280.e8.
42. Lu R, Zhao X, Li J, et al. Genomic characterisation and epidemiology of 2019 novel coronavirus: implications for virus origins and receptor binding. Lancet 2020;395(10224):565–574.
43. Xiao F, Tang M, Zheng X, Liu Y, Li X, Shan H. Evidence for Gastrointestinal Infection of SARS-CoV-2. Gastroenterology 2020;158(6):1831–1833.e3.
44. Cheung JC, Lam KN. POCUS in COVID-19: pearls and pitfalls. Lancet Respir Med 2020;8(5):e34.
45. Frates M. US imaging in the time of COVID-19. SRU Newsletter, 2020.
46. Dane B, Brusca-Augello G, Kim D, Katz DS. Unexpected Findings of Coronavirus Disease (COVID-19) at the Lung Bases on Abdominopelvic CT. AJR Am J Roentgenol 2020;215(3):603–606.
47. Bhayana R, Som A, Li MD, et al. Abdominal Imaging Findings in COVID-19: Preliminary Observations. Radiology 2020;297(1):E207–E215.
48. Chany C, Moscovici O, Lebon P, Rousset S. Association of coronavirus infection with neonatal necrotizing enterocolitis. Pediatrics 1982;69(2):209–214.
49. Moscovici O, Chany C, Lebon P, Rousset S, Laporte J. Association of coronavirus infection with hemorrhagic entercolitis in newborn infants [in French]. C R Seances Acad Sci D 1980;290(13):869–872.
50. Takifuji K, Terasawa H, Oka M, Sahara M, Hara T, Itoh H. Computerized tomography scan findings of a patient with severe enterocolitis associated with the coronavirus disease 2019: a case report. Research Square doi: https://doi.org/10.21203/rs.3.rs-21006/v1. Posted April 3, 2020. Accessed July 20, 2020.
51. Childers BC, Cater SW, Horton KM, Fishman EK, Johnson PT. CT Evaluation of Acute Enteritis and Colitis: Is It Infectious, Inflammatory, or Ischemic?: Resident and Fellow Education Feature. RadioGraphics 2015;35(7):1940–1941.
52. Baruah V, Bose S. Immunoinformatics-aided identification of T cell and B cell epitopes in the surface glycoprotein of 2019-nCoV. J Med Virol 2020;92(5):495–500.
53. Parry AH, Wani AH, Yaseen M. Acute Mesenteric Ischemia in Severe Coronavirus-19 (COVID-19): Possible Mechanisms and Diagnostic Pathway. Acad Radiol 2020;27(8):1190.
54. Levine MS, Scheiner JD, Rubesin SE, Laufer I, Herlinger H. Diagnosis of pneumoperitoneum on supine abdominal radiographs. AJR Am J Roentgenol 1991;156(4):731–735.
55. Xu L, Liu J, Lu M, Yang D, Zheng X. Liver injury during highly pathogenic human coronavirus infections. Liver Int 2020;40(5):998–1004.
56. Chai X, Hu L, Zhang Y, et al. Specific ACE2 Expression in Cholangiocytes May Cause Liver Damage After 2019-nCoV Infection. bioRxiv [preprint]. https://doi.org/10.1101/2020.02.03.931766. Posted February 4, 2020. Accessed June 17, 2020.
57. Li H, Liu SM, Yu XH, Tang SL, Tang CK. Coronavirus disease 2019 (COVID-19): current status and future perspectives. Int J Antimicrob Agents 2020;55(5):105951.
58. Zhao B, Ni C, Gao R, et al. Recapitulation of SARS-CoV-2 Infection and Cholangiocyte Damage with Human Liver Organoids. bioRxiv [preprint] https://doi.org/10.1101/2020.03.16.990317. Posted March 17, 2020. Accessed June 17, 2020.
59. Guan WJ, Ni ZY, Hu Y, et al. Clinical Characteristics of Coronavirus Disease 2019 in China. N Engl J Med 2020;382(18):1708–1720.
60. Chen N, Zhou M, Dong X, et al. Epidemiological and clinical characteristics of 99 cases of 2019 novel coronavirus pneumonia in Wuhan, China: a descriptive study. Lancet 2020;395(10223):507–513.
61. Bangash MN, Patel J, Parekh D. COVID-19 and the liver: little cause for concern. Lancet Gastroenterol Hepatol 2020;5(6):529–530.
62. Yang X, Yu Y, Xu J, et al. Clinical course and outcomes of critically ill patients with SARS-CoV-2 pneumonia in Wuhan, China: a single-centered, retrospective, observational study. Lancet Respir Med 2020;8(5):475–481 [Published correction appears in Lancet Respir Med 2020;8(4):e26.].
63. Wong SH, Lui RN, Sung JJ. Covid-19 and the digestive system. J Gastroenterol Hepatol 2020;35(5):744–748.
64. Medeiros AK, Barbisan CC, Cruz IR, et al. Higher frequency of hepatic steatosis at CT among COVID-19-positive patients. Abdom Radiol (NY) 2020;45(9):2748–2754.
65. Xu X, Chang XN, Pan HX, et al. Pathological changes of the spleen in ten patients with coronavirus disease 2019 (COVID-19) by postmortem needle autopsy [in Chinese]. Zhonghua Bing Li Xue Za Zhi 2020;49(6):576–582.
66. Li J, Li RJ, Lv GY, Liu HQ. The mechanisms and strategies to protect from hepatic ischemia-reperfusion injury. Eur Rev Med Pharmacol Sci 2015;19(11):2036–2047.
67. Palomar-Lever A, Barraza G, Galicia-Alba J, et al. Hepatic steatosis as an independent risk factor for severe disease in patients with COVID-19: A computed tomography study. JGH Open 2020. doi: 10.1002/jgh3.12395. Published online August 4, 2020. Accessed August 15, 2020.
68. Revzin MV, Scoutt L, Smitaman E, Israel GM. The gallbladder: uncommon gallbladder conditions and unusual

presentations of the common gallbladder pathological processes. Abdom Imaging 2015;40(2):385–399.
69. Ofosu A, Ramai D, Novikov A, Sushma V. Portal Vein Thrombosis in a Patient With COVID-19. Am J Gastroenterol 2020;115(9):1545–1546.
70. Low SW, Swanson KL, McCain JD, Sen A, Kawashima A, Pasha SF. Gastric ischemia and portal vein thrombosis in a COVID-19-infected patient. Endoscopy doi: 10.1055/a-1230-3357. Published online September 2, 2020. Accessed September 20, 2020.
71. Jafari SH, Naseri R, Khalili N, Haseli S, Bahmani M. Portal vein thrombosis associated with COVID-19: points to consider. BJR Case Rep 2020;6(3):20200089.
72. Franco-Moreno A, Piniella-Ruiz E, Montoya-Adarraga J, et al. Portal vein thrombosis in a patient with COVID-19. Thromb Res 2020;194:150–152.
73. Mohammadi S, Abouzaripour M, Hesam Shariati N, Hesam Shariati MB. Ovarian vein thrombosis after coronavirus disease (COVID-19) infection in a pregnant woman: case report. J Thromb Thrombolysis 2020;50(3):604–607.
74. Veyseh M, Pophali P, Jayarangaiah A, Kumar A. Left gonadal vein thrombosis in a patient with COVID-19-associated coagulopathy. BMJ Case Rep 2020;13(9):e236786.
75. Goldberg-Stein S, Fink A, Paroder V, Kobi M, Yee J, Chernyak V. Abdominopelvic CT findings in patients with novel coronavirus disease 2019 (COVID-19). Abdom Radiol (NY) 2020;45(9):2613–2623.
76. Liu F, Long X, Zhang B, Zhang W, Chen X, Zhang Z. ACE2 Expression in Pancreas May Cause Pancreatic Damage After SARS-CoV-2 Infection. Clin Gastroenterol Hepatol 2020;18(9):2128–2130.e2.
77. Wang F, Wang H, Fan J, Zhang Y, Wang H, Zhao Q. Pancreatic Injury Patterns in Patients With Coronavirus Disease 19 Pneumonia. Gastroenterology 2020;159(1):367–370.
78. Yang JK, Lin SS, Ji XJ, Guo LM. Binding of SARS coronavirus to its receptor damages islets and causes acute diabetes. Acta Diabetol 2010;47(3):193–199.
79. Richardson S, Hirsch JS, Narasimhan M, et al. Presenting Characteristics, Comorbidities, and Outcomes Among 5700 Patients Hospitalized With COVID-19 in the New York City Area. JAMA 2020;323(20):2052–2059 [Published correction appears in JAMA 2020;323(20):2098.].
80. Ronco C, Reis T, Husain-Syed F. Management of acute kidney injury in patients with COVID-19. Lancet Respir Med 2020;8(7):738–742.
81. Petrilli CM, Jones SA, Yang J, et al. Factors associated with hospital admission and critical illness among 5279 people with coronavirus disease 2019 in New York City: prospective cohort study. BMJ 2020;369:m1966.
82. Cummings MJ, Baldwin MR, Abrams D, et al. Epidemiology, clinical course, and outcomes of critically ill adults with COVID-19 in New York City: a prospective cohort study. Lancet 2020;395(10239):1763–1770.
83. Hirsch JS, Ng JH, Ross DW, et al. Acute kidney injury in patients hospitalized with COVID-19. Kidney Int 2020;98(1):209–218.
84. Argenziano MG, Bruce SL, Slater CL, et al. Characterization and clinical course of 1000 Patients with COVID-19 in New York: retrospective case series. medRxiv [preprint]. https://doi.org/10.1101/2020.04.20.20072116. Posted May 7, 2020. Accessed June 15, 2020.
85. Zhou F, Yu T, Du R, et al. Clinical course and risk factors for mortality of adult inpatients with COVID-19 in Wuhan, China: a retrospective cohort study. Lancet 2020;395(10229):1054–1062 [Published correction appears in Lancet 2020;395(10229):1038.].
86. Cummings MJ, Baldwin MR, Abrams D, et al. Epidemiology, clinical course, and outcomes of critically ill adults with COVID-19 in New York City: a prospective cohort study. Lancet 2020;395(10239):1763–1770.
87. Batlle D, Soler MJ, Sparks MA, et al. Acute Kidney Injury in COVID-19: Emerging Evidence of a Distinct Pathophysiology. J Am Soc Nephrol 2020;31(7):1380–1383.
88. Pan XW, Xu D, Zhang H, Zhou W, Wang LH, Cui XG. Identification of a potential mechanism of acute kidney injury during the COVID-19 outbreak: a study based on single-cell transcriptome analysis. Intensive Care Med 2020;46(6):1114–1116.
89. Basara Akin I, Altay C, Eren Kutsoylu O, Secil M. Possible radiologic renal signs of COVID-19. Abdom Radiol (NY) doi: 10.1007/s00261-020-02671-8. Published online July 28, 2020. Accessed August 15, 2020.
90. Li MY, Li L, Zhang Y, Wang XS. Expression of the SARS-CoV-2 cell receptor gene ACE2 in a wide variety of human tissues. Infect Dis Poverty 2020;9(1):45.
91. Wang S, Zhou X, Zhang T, Wang Z. The need for urogenital tract monitoring in COVID-19. Nat Rev Urol 2020;17(6):314–315.
92. Chen Y, Feng Z, Diao B, et al. The Novel Severe Acute Respiratory Syndrome Coronavirus 2 (SARS-CoV-2) Directly Decimates Human Spleens and Lymph Nodes. medRxiv [preprint] doi: https://www.medrxiv.org/content/10.1101/2020.03.27.20045427v.1 Posted March 31, 2020. Accessed June 17, 2020.
93. Santos Leite Pessoa M, Franco Costa Lima C, Farias Pimentel AC, Godeiro Costa JC, Bezerra Holanda JL. Multisystemic Infarctions in COVID-19: Focus on the Spleen. Eur J Case Rep Intern Med 2020;7(7):001747.
94. Suwanwongse K, Shabarek N. Rhabdomyolysis as a Presentation of 2019 Novel Coronavirus Disease. Cureus 2020;12(4):e7561.
95. Jin M, Tong Q. Rhabdomyolysis as Potential Late Complication Associated with COVID-19. Emerg Infect Dis 2020;26(7):1618–1620.
96. Zutt R, van der Kooi AJ, Linthorst GE, Wanders RJ, de Visser M. Rhabdomyolysis: review of the literature. Neuromuscul Disord 2014;24(8):651–659.
97. Melli G, Chaudhry V, Cornblath DR. Rhabdomyolysis: an evaluation of 475 hospitalized patients. Medicine (Baltimore) 2005;84(6):377–385.
98. Cunningham J, Sharma R, Kirzner A, et al. Acute myonecrosis on MRI: etiologies in an oncological cohort and assessment of interobserver variability. Skeletal Radiol 2016;45(8):1069–1078.
99. Moratalla MB, Braun P, Fornas GM. Importance of MRI in the diagnosis and treatment of rhabdomyolysis. Eur J Radiol 2008;65(2):311–315.
100. Magro C, Mulvey JJ, Berlin D, et al. Complement associated microvascular injury and thrombosis in the pathogenesis of severe COVID-19 infection: A report of five cases. Transl Res 2020;220:1–13.
101. Galván Casas C, Català A, Carretero Hernández G, et al. Classification of the cutaneous manifestations of COVID-19: a rapid prospective nationwide consensus study in Spain with 375 cases. Br J Dermatol 2020;183(1):71–77.
102. Alramthan A, Aldaraji W. Two cases of COVID-19 presenting with a clinical picture resembling chilblains: first report from the Middle East. Clin Exp Dermatol 2020;45(6):746–748.
103. Manalo IF, Smith MK, Cheeley J, Jacobs R. A dermatologic manifestation of COVID-19: Transient livedo reticularis. J Am Acad Dermatol 2020;83(2):700.
104. Wu P, Duan F, Luo C, et al. Characteristics of Ocular Findings of Patients With Coronavirus Disease 2019 (COVID-19) in Hubei Province, China. JAMA Ophthalmol 2020;138(5):575–578.
105. Stokes EK, Zambrano LD, Anderson KN, et al. Coronavirus Disease 2019 Case Surveillance: United States, January 22-May 30, 2020. MMWR Morb Mortal Wkly Rep 2020;69(24):759–765.
106. Centers for Disease Control and Prevention. Coronavirus Disease 2019 (COVID-19): Information for Pediatric Health Care Providers. https://www.cdc.gov/coronavirus/2019-ncov/hcp/pediatric-hcp.html. Updated August 19, 2020. Accessed September 20, 2020.
107. Kim L, Whitaker M, O'Halloran A, et al. Hospitalization Rates and Characteristics of Children Aged <18 Years Hospitalized with Laboratory-Confirmed COVID-19: COVID-NET, 14 States, March 1-July 25, 2020. MMWR Morb Mortal Wkly Rep 2020;69(32):1081–1088.
108. Liu Y, Yan LM, Wan L, et al. Viral dynamics in mild and severe cases of COVID-19. Lancet Infect Dis 2020;20(6):656–657.

109. Dong XC, Li JM, Bai JY, et al. Epidemiological characteristics of confirmed COVID-19 cases in Tianjin [in Chinese]. Zhonghua Liu Xing Bing Xue Za Zhi 2020;41(5):638–641.
110. Poline J, Gaschignard J, Leblanc C, et al. Systematic SARS-CoV-2 screening at hospital admission in children: a French prospective multicenter study. Clin Infect Dis 2020. 10.1093/cid/ciaa1044. Published online July 25, 2020. Accessed August 15, 2020.
111. Hoang A, Chorath K, Moreira A, et al. COVID-19 in 7780 pediatric patients: a systematic review. EClinicalMedicine 2020;24:100433.
112. Götzinger F, Santiago-García B, Noguera-Julián A, et al. COVID-19 in children and adolescents in Europe: a multinational, multicentre cohort study. Lancet Child Adolesc Health 2020;4(9):653–661.
113. Xia W, Shao J, Guo Y, Peng X, Li Z, Hu D. Clinical and CT features in pediatric patients with COVID-19 infection: Different points from adults. Pediatr Pulmonol 2020;55(5):1169–1174.
114. Chan SS, Kotecha MK, Rigsby CK, et al. ACR Appropriateness Criteria: Pneumonia in the Immunocompetent Child. Reston, Va: American College of Radiology, 2019.
115. Foust AM, Phillips GS, Chu WC, et al. International Expert Consensus Statement on Chest Imaging in Pediatric COVID-19 Patient Management: Imaging Findings, Imaging Study Reporting and Imaging Study Recommendations. Radiol Cardiothorac Imaging https://doi.org/10.1148/ryct.2020200214. Published Apirl 23, 2020. Accessed August 15, 2020.
116. Riphagen S, Gomez X, Gonzalez-Martinez C, Wilkinson N, Theocharis P. Hyperinflammatory shock in children during COVID-19 pandemic. Lancet 2020;395(10237):1607–1608.
117. Jones VG, Mills M, Suarez D, et al. COVID-19 and Kawasaki Disease: Novel Virus and Novel Case. Hosp Pediatr 2020;10(6):537–540.
118. Harahsheh AS, Dahdah N, Newburger JW, et al. Missed or delayed diagnosis of Kawasaki disease during the 2019 novel coronavirus disease (COVID-19) pandemic. J Pediatr 2020;222:261–262.
119. Hameed S, Elbaaly H, Reid CEL, et al. Spectrum of Imaging Findings on Chest Radiographs, US, CT, and MRI Images in Multisystem Inflammatory Syndrome in Children (MIS-C) Associated with COVID-19. Radiology doi: 10.1148/radiol.2020202543. Published online June 25, 2020. Accessed August 15, 2020.
120. Verdoni L, Mazza A, Gervasoni A, et al. An outbreak of severe Kawasaki-like disease at the Italian epicentre of the SARS-CoV-2 epidemic: an observational cohort study. Lancet 2020;395(10239):1771–1778.
121. Whittaker E, Bamford A, Kenny J, et al. Clinical Characteristics of 58 Children With a Pediatric Inflammatory Multisystem Syndrome Temporally Associated With SARS-CoV-2. JAMA 2020;324(3):259–269.
122. Sadiq M, Aziz OA, Kazmi U, et al. Multisystem inflammatory syndrome associated with COVID-19 in children in Pakistan. Lancet Child Adolesc Health 2020;4(10):e36–e37.
123. Rasmussen SA, Smulian JC, Lednicky JA, Wen TS, Jamieson DJ. Coronavirus Disease 2019 (COVID-19) and pregnancy: what obstetricians need to know. Am J Obstet Gynecol 2020;222(5):415–426.
124. Rasmussen SA, Jamieson DJ. Coronavirus Disease 2019 (COVID-19) and Pregnancy: Responding to a Rapidly Evolving Situation. Obstet Gynecol 2020;135(5):999–1002.
125. Lam CM, Wong SF, Leung TN, et al. A case-controlled study comparing clinical course and outcomes of pregnant and non-pregnant women with severe acute respiratory syndrome. BJOG 2004;111(8):771–774.
126. Breslin N, Baptiste C, Gyamfi-Bannerman C, et al. Coronavirus disease 2019 infection among asymptomatic and symptomatic pregnant women: two weeks of confirmed presentations to an affiliated pair of New York City hospitals. Am J Obstet Gynecol MFM 2020;2(2):100118.
127. Liu D, Li L, Wu X, et al. Pregnancy and Perinatal Outcomes of Women With Coronavirus Disease (COVID-19) Pneumonia: A Preliminary Analysis. AJR Am J Roentgenol 2020;215(1):127–132.
128. Schnettler WT, Al Ahwel Y, Suhag A. Severe acute respiratory distress syndrome in coronavirus disease 2019-infected pregnancy: obstetric and intensive care considerations. Am J Obstet Gynecol MFM 2020;2(3):100120.
129. Chen H, Guo J, Wang C, et al. Clinical characteristics and intrauterine vertical transmission potential of COVID-19 infection in nine pregnant women: a retrospective review of medical records. Lancet 2020;395(10226):809–815 [Published correction appears in Lancet 2020;395(10229):1038.].
130. Penfield CA, Brubaker SG, Limaye MA, et al. Detection of severe acute respiratory syndrome coronavirus 2 in placental and fetal membrane samples. Am J Obstet Gynecol MFM 2020;2(3):100133.
131. Baud D, Greub G, Favre G, et al. Second-Trimester Miscarriage in a Pregnant Woman With SARS-CoV-2 Infection. JAMA 2020;323(21):2198–2200.
132. Lu Q, Shi Y. Coronavirus disease (COVID-19) and neonate: What neonatologist need to know. J Med Virol 2020;92(6):564–567.
133. Wu X, Sun R, Chen J, Xie Y, Zhang S, Wang X. Radiological findings and clinical characteristics of pregnant women with COVID-19 pneumonia. Int J Gynaecol Obstet 2020;150(1):58–63.